Gravel Barrier Beach Morphodynamic Response to Storm Events

Kristian David Ions BEng (Hons)

Submitted to Swansea University in fulfilment of the requirements for the Degree of master's by Research.

Swansea University 2020.

Acknowledgement

Abstract

Gravel beaches and barriers form a valuable natural protection for many shorelines. Gravel beach response to waves has been studied extensively, for regular and irregular waves, but there is little reported investigation of beach response to bimodal wave conditions, quite commonly experienced at midlatitudes. The paper presents a numerical modelling study of gravel barrier beach response to storm wave conditions. The XBeach non-hydrostatic model was set up in 1D mode to investigate barrier volume change and overwash under a wide range of unimodal and bimodal storm conditions and barrier cross sections. The numerical model was validated against conditions at Hurst Castle Spit, UK. The validated model is used to simulate the response of a range of gravel barrier cross sections under a wide selection of statistically significant storm wave and water level scenarios thus simulating an ensemble of realisations of barrier volume change and overwash. This ensemble of results was used to develop a simple parametric model for estimating barrier volume change during a given storm and water level condition. Attempts were also made to model overwash and crest changes of barriers, however further study Is required. Numerical simulations of barrier response to bimodal storm conditions, which are a common occurrence in many parts of the UK, reveals that barrier volume change and overwash from bimodal storms will be higher than that from unimodal storms if the swell percentage is greater than 40%. The limitations of the modelling approach and the model results are noted. The model is demonstrated as providing a useful tool for estimating barrier volume change, a commonly used measure used in gravel barrier beach management.

Table of Contents

List of Tables

List of Figures

Declarations

This work has not previously been accepted in substance for any degree and is not being concurrently submitted in candidature for any degree.

Signed... ██████████████████████████████ ....

Date.......…22/12/2020..……

This thesis is the result of my own investigations, except where otherwise stated. Other sources are acknowledged by footnotes giving explicit references. A bibliography is appended.

Signed…. ██████████████████████████ ....

Date.........22/12/2020...

I hereby give my consent for my work, if relevant and accepted, to be available for photocopying and for inter-library loans **after expiry of a bar on access approved by the University.**

Signed.. ██████████████████████████ ....

Date......22/12/2020..
....

1. Introduction

Gravel beaches and barriers form a significant proportion of world's beaches at mid to high latitudes (Carter and Orford, 1993). They act as natural means of coast protection and are capable of dissipating a large portion of incident wave energy under highly energetic wave conditions (Aminti et al., 2003; Buscombe and Masselink, 2006). Gravel beach and barrier morphodynamics are dominated by the highly reflective nature of steep beach face, energetic swash motions generated by waves breaking on the lower shoreface and potential overwash of the beach crest (Almeida et al., 2014). Overwashing and overtopping of gravel beaches and barriers can occur during extreme storm conditions and can lead to crest build-up, crest lowering, landward retreat and, maybe, breaching (Carter and Orford 1993; Bradbury and Powell, 1992; Bradbury et al., 2005). Pressures of sea level rise and increased storminess associated with global climate change may lead to frequent overwashing and even breaching, hence diminishing their natural coast protection function.

Bimodal storm conditions are also known to pose significant risk to existing coastal defences designed for Unimodal conditions (Bradbury et al., 2007) with bimodal wave conditions increasing the run-up and overwashing over defences considerably (Masselink et al., 2014). It is well known that the south-west of the UK is subjected to frequent storms with bimodal characteristics as a result of swell-dominated waves reaching from the Atlantic. Bradbury et al. (2007) found that bimodal conditions occur 25% of time during winter months where storms are frequent. Nicholls and Webber (1989), Thompson et al. (2018) and some others reveal that bimodal storms may induce greater beach erosion and damage than their unimodal counterparts at certain occasions.

Studies of gravel beach and barrier morphodynamics date back to a few decades. Powel (1988) investigated the hydraulic behaviour of gravel beaches using a set of physical model testing results. Following that, Powel (1990) presented a parametric model for gravel beach morphodynamic evolution against short term wave attack, based on a comprehensive series of physical model tests. The application of his model to several field sites proved it to be a useful tool to determine short term cross-shore profile evolution of gravel beaches. However, Powell's (1990) model does not consider barrier overwash thus limiting its application to ordinary wave conditions. Bradbury (2000) investigated a relationship between incident wave conditions and the geometry of barrier beaches under storm wave conditions using an extensive series of physical model experimental results on cross-shore profile change of gravel beaches. He then developed an empirical framework of dimensionless threshold called 'barrier inertia parameter', which is a function of emergent barrier

cross-sectional area, free board and the incident wave height, to detect barrier beaching. Bradbury et al. (2005) applied Bradbury (2000) empirical framework in predictive mode to investigate the morphodynamic response of a number of barrier beaches in the southern England. The barrier inertia parameter is found to be a useful tool to identify incident wave conditions leading to barrier beach, although the range of validity of it is limited to incident wave steepness below a certain value. The extrapolation of the parameter to higher incident wave steepness has found to be problematic and unreliable.

Most investigations on gravel beach and barrier overwash and morphodynamics found in literature are based on either experimental investigations (e.g. Powell, 1986, 1990; Van-Rijn & Sutherland, 2011; Bradbury 2000; Roman-Blanco et al., 2006; Matias et al, 2012; Matias, 2014; Polidoro et al., 2018) or field studies (e.g. Orfed and Carter, 1993; Chadwick et al., 2005; Buscombe and Masselink, 2006; Austin and Buscombe, 2008; Ruiz de Alegria-Arzaburu and Masselink, 2010; Almeida et al., 2014 and some others). Some attempts have been made to apply numerical models to simulate morphodynamic response to incident waves and water levels. Williams et al. (2012) used XBeach, the process-based coastal morphodynamic model (Roelvink et al., 2009) to investigate overwashing and breaching of a cross-shore profile of a gravel barrier located in a macrotidal environment in the south-west coast of the UK. They had some success but, the model over-predicted the erosion of the upper beach face although the model was able to identify the threshold water level and wave conditions for overwashing. Jamal et al. (2014) modified the XBeach model to investigate the morphodynamic behaviour of gravel beaches by introducing a coarse sediment transport formula and groundwater infiltration/exfiltration phenomena. The modified model (XBeach v12) was found to capture gravel transport and beach morphodynamics satisfactorily. McCall et al. (2015) also presented an extension to XBeach to simulate morphodynamics of gravel beaches. This model, called XBeach-G,is capable of capturing morphodynamic responses of gravel beaches ranging from berm building to roll-over of gravel barriers. Garagozlou et al. (2020) used XBeachX to simulate overwash, erosion and breach of barrier islands during extreme storm conditions. Philips et al. (2020) used XBeach non-hydrostatic (XBeach-X) model to study intertidal foreshore evolution and runup of gravel barriers. They concluded that the sandy intertidal area in their study site plays an important role in runup and overwash of gravel barriers.

Although process-based models are useful tools to investigate gravel beach and barrier response to extreme conditions, establishing a high-resolution numerical model to a given site can be time-consuming and costly. Also, significant uncertainties surround deterministic simulations due to uncertain input parameters and inadequate process-descriptions in those models thus requiring a

large number of simulations. Therefore, the application of these models may have limited scope within the coastal engineering industry where time and resources are restricted and expensive. Also, trends of variability of gravel beaches may be more important for coastal management decision making than a single deterministic prediction of beach change without uncertainty quantifications.

The Main objectives of the thesis are to:

- Calibrate and validate a process-based numerical model to the selected field site of a gravel barrier beach
- Model morphodynamic response of the gravel barrier to extreme hydrodynamic conditions under both Unimodal and Bimodal waves of varying return periods derived by Bradbury et al, (2005) on multiple cross sections of Hurst Spit
- Investigate and describe the gravel barrier response to varying wave conditions
- Develop a parametric model to estimate gravel barrier morphodynamic response to extreme conditions
- Investigate the impacts of incident bimodality on gravel barrier morphodynamic response

This study aimed at addressing two research needs identified in literature: (i) Although process-based models are useful tools to investigate gravel beach and barrier response to extreme conditions, establishing a high-resolution numerical model to a given site can be time-consuming and costly. Also, significant uncertainties surround deterministic simulations due to uncertain input parameters and inadequate process-descriptions in those models thus requiring a large number of simulations to quantify uncertainties. Therefore, the application of these models may have limited scope within the coastal engineering industry where time and resources are restricted and expensive; (ii) Simple gravel barrier models have their own limitations: Powell (1988) parametric model is not able to capture barrier overwash. The barrier inertia parameter defined by Bradbury et al. (2005) links barrier inertia into breaching thresholds but does not capture morphodynamic change. Poate et al. (2016) was successful with an attempt to parameterise wave runup on a gravel beach but did not investigate gravel barrier morphodynamics.

Critical to this is the ultimate objective for practitioners to make sustainable long-term decisions on the management of these systems. As the climate continues to change, multiple questions arise that require consideration for coastal managers. E.g., when is failure/breaching likely should management

cease? Can this system function effectively as flood/erosion protection in the future? How might the barrier have to be adapted to continue to manage risk? Are long-term adaptation requirements technically and economically feasible? In the UK, the above type of decision making is typically made assuming a 100-year period for new interventions. Given the inherent uncertainty in all aspects of this process it is important that coastal engineers have tools available that can quickly support decision making on the critical aspects and provide focus for more detailed studies if required.

The first part of this thesis will address the need to develop a simple parametric model to capture gravel barrier beach morphodynamic response to extreme conditions. The second part is devoted to gravel barrier response to bimodal storm conditions.

2. Background and Literature Review

In this section a brief description of nearshore process relevant to the study and a review of literature relating to the gravel barrier beaches are given

2.1 Surf Zone Processes

Ocean waves are mostly generated by wind force on the water's surface. Waves can travel thousands of miles, known as fetch, with little decrease in wave height, whilst maintaining wave period (Reeve & Chadwick, 2018). Waves are formed with different frequencies resulting in wave dispersion, and therefore reach the shoreline at varying time. As the waves approach the shoreline, seabed friction forces effect the wave height and wavelength through shoaling and refraction processes. As waves begin to break there is significant rates of change in momentum in the fluid, resulting in radiation stresses, where the horizontal component is responsible for long shore currents, and cross shore component is responsible for wave set-up, both these processes are discussed in greater detail below Wave breaking occurs at initial break point where wave height is *Hb*, at angle α_β to the beach. The wave breaking process are complex, a brief overview is given below (Reeve & Chadwick, 2018).

2.1.1 Wave Breaking

Refraction occurs when waves travel from deeper water to shallow water depths, where seabed friction results in decrease in wave celerity and therefore change in wave angle of attack:

$$\frac{sin\alpha}{sin\alpha_0} = \frac{L}{L_0} = \frac{c}{c_0} = \tanh{(kh)} \qquad\qquad (1.0)$$

where α is shallow water wave angle, α_0 is wave angle in deep water, L is shallow water wavelength, L_0 is deep water wavelength, c is shallow water wave celerity, c_0 is deep water wave celerity, k is the wave number and h is water depth. As a result of wave refraction the angle of wave attack is altered, which can cause wave focusing on certain parts of shoreline (Bradbury & Powell, 1993).

Shoaling is the process of wave steepening until its point of breaking due to friction forces from seabed:

$$\frac{H}{H_0} = \left(\frac{c_{go}}{c_g}\right)^{\frac{1}{2}} = K_s \qquad\qquad (1.1)$$

where H is the shallow water wave height, H_0 is deep water wave height, c_{go} is the deep-water wave group celerity, c_g is the shallow water wave group celerity and K_s is the shoaling co-efficient.

Two main criteria determine wave breaking and location, these are steepness of the wave front (H_s/L_m), H_s is significant wave height and L_m is wavelength. The second is the depth of water the wave propagates in, known as the breaker index. A general rule is wave breaking will occur when $h_b = 1.28H_b$ (Reeve & Chadwick, 2018) where h_b is depth of water where waves break and H_b is wave breaking height.

Using the wave breaker index $\gamma = \frac{H}{h}$, where H is wave height and h is water depth, (Goda & Takagi, 2000) developed a design diagram for wave breaker limits, derived through wave laboratory experiments using the relationship between $\frac{H_b}{L_0}$, where L_0 is deep water wave height.

There are three types of wave breakers, defined by the Iribarren number:

$$\xi_b = \frac{tan\beta}{\sqrt{H_b/L_m}} \qquad\qquad (1.2)$$

where $tan\beta$ is beach slope.

Spilling breakers are very flat beach slopes where $\xi_b < 0.4$.

Plunging breakers have steep beach slopes where $0.4 \leq \xi_b \leq 2.0$.

Surging breakers are very steep beach slopes where $\xi_b > 2.0$.

Wave set down or set up is a process where surface water level increases or decreases relative to the still water level. The process occurs due to onshore momentum flux , S_{xx}, needing to be balanced by and equal and opposite force. In general wave set-down is less than 5% of breaking water depth, whereas wave setup is approximately 20-30% of water breaking depth. Wave set up can contribute to overtopping of structures (Reeve & Chadwick, 2018).
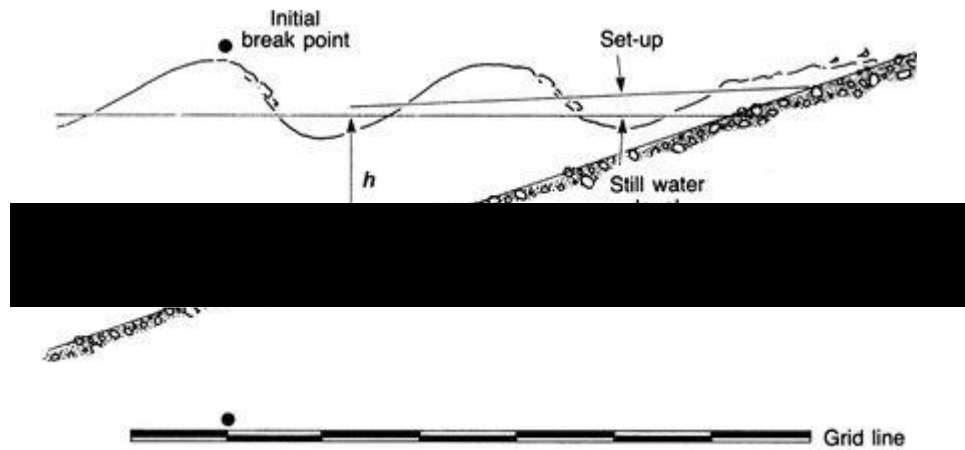
Figure 1.0- Diagram of Wave set up and set down (Reeve & Chadwick, 2018)*.*

The onshore momentum flux is categorised as Radiation stresses, S_{xx} , S_{yy}. They arise from the orbital motion of water particles, producing forces in the S_{xx} , S_{yy} directions (M.S. Longuet-Higgins, 1964). Where θ is wave angle.

$$S_{xx} = S_{xx} \cos^2 \theta + S_{yy} \sin^2 \theta \qquad (1.3)$$

$$S_{yy} = S_{xx} \sin^2 \theta + S_{yy} \cos^2 \theta \qquad (1.4)$$

$$S_{xy} = S_{xx} \sin \theta cos\theta + S_{yy} sin\theta \cos \theta \qquad (1.5)$$

Radiation stresses has been used to explained longshore transport currents through S_{xy} in the surf zone. Outside the surf zone there is no external force driving longshore currents. Longshore effects

17

can have large impacts on beach morphology long term; however, the focus of this study is purely cross shore processes.

2.1.2 Sediment Transport

Sediment transport processes are described below through the main underlying principles. The two principles of transport are either by rolling, sliding, or bouncing of particles on top of other particles- this is known as bedload, or by suspension of sediment in the moving fluid, known as suspended load. An extension of bedload transport which are of less significance in the study of gravel sized sediment is sheet flow, where large amounts of sediment are transported via many layers of bedload sediment. Sediment is transported when the bed shear stress on the particle τ_0 is sufficiently large, where an increase in horizontal fluid velocity u, results in larger τ_0 values (Reeve & Chadwick, 2018).

$$\tau_0 = \tau_{0s} + \tau_{0f} + \tau_{0t} \qquad (1.6)$$

Where τ_{0s} is skin friction, τ_{0f} is form drag, τ_{0t} is the sediment transport contribution caused by momentum transfer.

The Shields parameter, also known as the entrainment function, derived through experimental data, relating Reynolds number to critical entrainment function (Shields, 1936) known as the shields parameter:

$$\theta = \frac{\tau}{(p_s - p)gD} \qquad (1.7)$$

at the moment shear force is sufficiently large to mobilise particle θ is expressed as:

$$\theta_{cr} = \frac{\tau_{cr}}{(p_s - p)gD} \qquad (1.8)$$

the relationship was later refined by Soulsby (1997). Critical shields parameter is given by:

$$\theta_{cr} = \frac{0.3}{1 + 1.2D_*} + 0.055[1 - \exp(-0.02D_*)] \qquad (1.9)$$

$$\text{where } D_* = \left[\frac{g(s-1)}{v^2}\right]^{\frac{1}{3}} \qquad (1.10)$$

building on shields initial work, sediment transport is related to shields parameter:

$$\Phi = q_b / [g(s-1)D^3]^{\frac{1}{2}} \qquad (1.11)$$

18

where q_b is bedload transport rate (m³/m/s). There have been several other successful adaptations of this formulae such as Meyer-Peter Muller (1957) and Nielsen (1992). Bedload transport is known to be the predominate process on gravel beaches (Reeve & Chadwick, 2018). Other notable sediment transport formulae are (Van Rijn, 2007;Van Rijn, 1987:McCall-Van-Rijn 2015).

2.1.3 Wave Spectrum

In order to classify the local wave climate, a statistical approach is taken obtaining design conditions. Commonly in coastal engineering the Joint North Sea Wave Observation Project (JONSWAP) Spectrum (Hasselmann et al., 1973) is used to force wave conditions into numerical models and classify the sea state. The spectrum quantifies the wave height, wave period and wave propagation angle. generated Local wind waves are characterised by Unimodal wave conditions, the JONSWAP has a single peak frequency, with one wave height and one peak wave period. For Bimodal wave conditions there is a double peaked JONSWAP spectrum formed by the superposition of swell waves and local wind waves (Orimoloye et al., 2019). Swell wave categorised as waves generated outside of the local climate which are no longer affected by local winds.
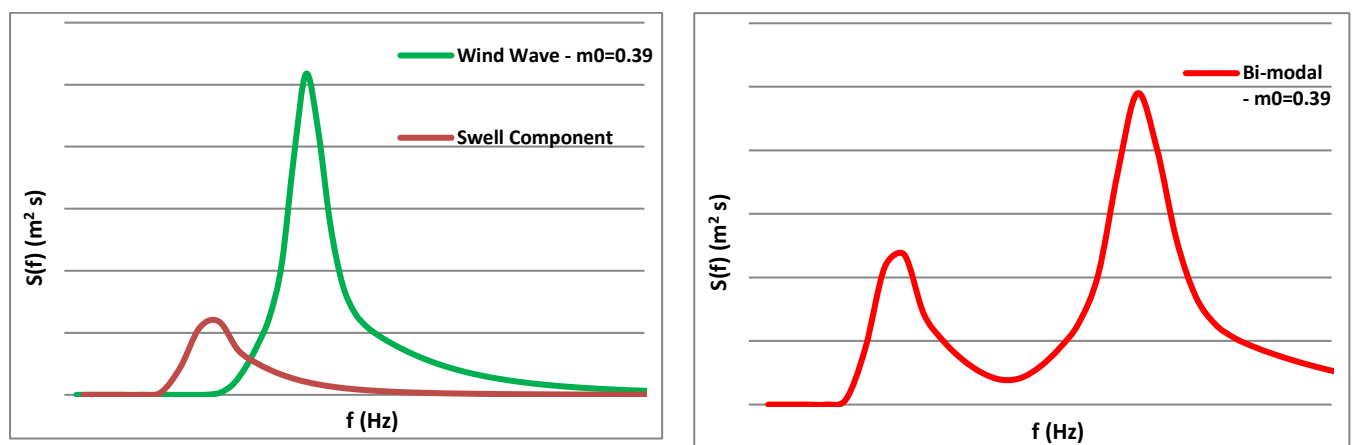
Figure 1.1- Left Figure- Green line represents Wind wave Unimodal Spectrum, brown line represents swell wave unimodal spectrum. Right Figure – Shows the Bimodal Spectrum of superposition wind and swell waves. Spectrums developed using Polidoro et al. 2014.

2.2 Gravel beach dynamics
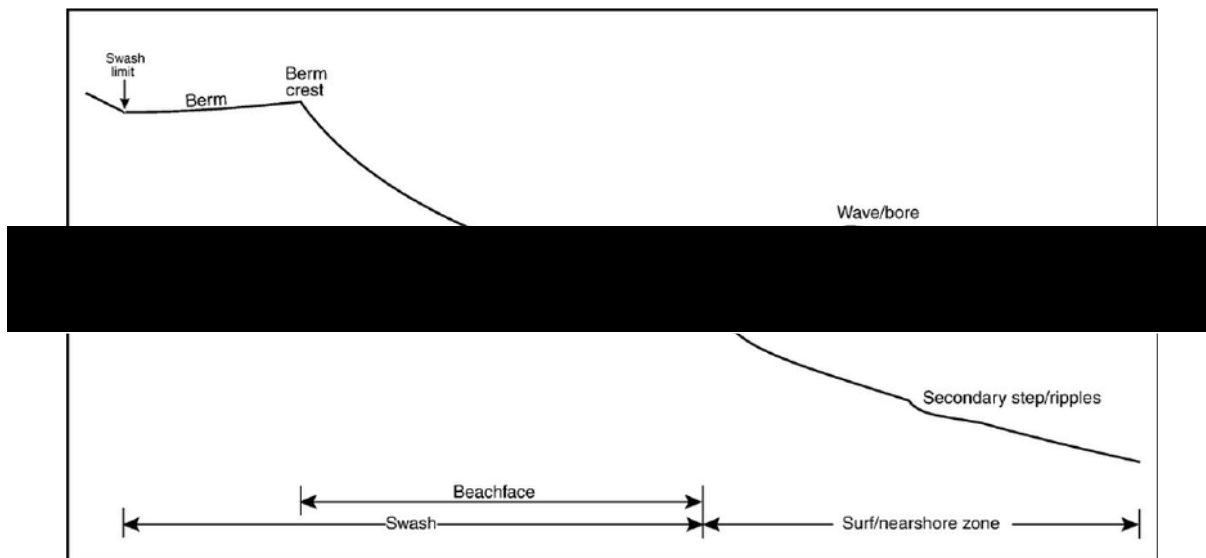
Figure 1.2- Schematisation of gravel beaches (Austin & Masselink, 2006).

Gravel beaches have several key defining features, they have steep beach faces, typically in order of 1:5 slope (Reeve & Chadwick, 2018), due to the large sediment size, ranging from 10mm-40mm. Despite the larger sediment sizes, large net sediment transport is very common. The steeper beach faces result in a much more reflective nature when compared to sandy beaches (Austin & Masselink, 2006), as well as wave attack propagating closer to the shoreline, resulting in a plunging breaker (Reeve & Chadwick, 2018), this is in contrast to the gradual breaking slope found on sandy beaches which results in much wider surf zone with wave breaking much further offshore (Lorang, 2002).Due to the plunging breaker the surf zone is very narrow, often as wide as the swash zone, meaning the swash zone is of much greater importance in gravel beaches(Austin & Masselink, 2006), dominated by incident-band motions, with limited development of infragravity motion waves. There is also increased chance of significant wave grouping till shoreline, which results in large breakpoint focusing and concentration of energy on the shoreline, this in turn means transport thresholds are always nearly exceeded during storms (Carter and Orford, 1993). Due to larger sediment sizes sediment transport on gravel beaches is mostly bed load and sheet flow (Austin & Masselink, 2006), whilst suspended sediment is not of importance due to higher settling velocity of gravel particles.

 Another defining feature of gravel beaches are the permeability, typically ranging from $1.10^{-3} - 1 \, ms^{-1}$ (López De San & Blanco, 2003;McCall et al., 2015). The porous nature of gravel beaches is known to have large impact on the morphology on gravel beaches(Li, 1997; Lee, 2007). Due to large sediment sizes, higher potential infiltration during uprush results in larger sediment being deposited further up the beach face, which in terms leads to the creation of the berm. Lee (2007) found that the

berm formed in the upper portion of the shoreline and moves up the beach as the groundwater level falls and the lower the groundwater level, the steeper the beach surface. The effect of infiltration loses and saturation of gravel beaches can be classified into 2 sub categories; Reduction of backwash, in which Masselink & Li (2001) found significant net sediment transport would be impacted for sediment diameter greater than 0.5mm; The second effect is an increase in vertical pressure gradients and boundary layer ventilation.

The berm is marked as a sudden change in beach slope, controlled by both the sea water level and wave attack. As the still water level increase the berm is found higher up the beach face. During calmer conditions, sediment lenses are formed as wave deposit sediment over multiple tidal cycles on the upper beach face creating the berm. There can often be multiple, parallel berms found on the beach face, deposited by different wave energies over time (Austin & Masselink, 2006b). During large storm events the berm are often destroyed. Another key morphological feature of gravel beaches is the step, which is formed at the foot of the beach forming a distinct break slope, that acts as a dissipative breakwater for oncoming wave attack. The step controls the location of wave breaking on the beach, and although is not a feature of the swash zone, the Morphodynamics processes of the step are just as important to beach morphology (McCall et al., 2015). When there are higher astronomical tides or storm surges the step migrates further up the beach, therefore advancing the point of wave attack. This reduces the width of the beach and results in greater run up of beaches and barriers (Bradbury, 2000).

Barrier beaches are another common form of natural coastal defence, they are narrow ridges of sand or gravel. They generally are found to run parallel to shore, separated by lagoons, marshlands and tidal flats which offer areas of marine, and ecological conservation sites (Reeve & Chadwick, 2018). Short term response of barrier beaches is controlled by local wave climate, astronomical tidal variations and storm surges, barrier pre-storm geometry and geology. Barrier beach long term morphology is linked to rising sea levels, resulting in net landward migration of the barrier due to overtopping processes (Bradbury, 2000;Dubois, 1990). A Previous study by Powell (1990) stated that for any given number of waves a dynamic equilibrium will be reached, provided there is no overwash occurring. However, the reality of barrier beaches is that overwashing occurs and dictates both short term and long-term morphology. Overtopping occurs when the run up height exceeds that of the barrier crest above the still water level(Bradbury, 2000; Sallenger , 2000), resulting in sediment deposition on the back of the barrier. Over time this then results in the landward migration of the barrier during storm events, and storm sequencing as the sediment that is overwashed is effectively lost from the system, with no means of natural re-nourishment. Previous study by Powell(1990) stated

that for any given number of waves a dynamic equilibrium will be reached, provided there is no overwash occurring.

There are 4 distinctive barrier beach processes, (Carter, 1993; Orford, 1995) there are:

- Crest build up-due to overtopping and sediment deposit on barrier crest
- Crest lowering-due to overwashing events and sediment depositing on back of barrier
- Crest rollback-due to overwashing events
- Crest breaching-due to inundation of barrier

As the above processes are largely determined by wave over topping and overwashing, the still water level is of significant importance. Another key aspect of this study will be storm surges Storm conditions can cause the water level to increase above estimated tidal elevation. Storms in the UK are formed by low-pressure weather systems, which move rapidly across the ocean's surface and wind speeds are significantly increased due to storms. Storm surge variations are formed through combination of local barometric effect and the kinematic effect due to the moving storm system, and a dynamic effect of wind-stress on surface water (Reeve & Chadwick, 2018). Large storm surges occurring at mesotidal and microtidal scale locations during a 1/50 year storm can increase astronomical tidal range by 50% (Nicholls & Webber, 1989).These larger surges result in decreased crest height, as Sallenger (2000) presented, when freeboard decreases, overtopping increases.

2.3 Models for Morphodynamic changes

2.3.1 Conceptual Models

Conceptual models are useful in coastal management to gain a quick insight into to potential morphological changes on barrier beaches, however they do not offer a means of real prediction or quantitively estimating change. Early studies of gravel barriers were based of physical observations such as (Carter et al., 1993; Dubois, 1990; Orford et al., 1995). These studies researched closely the observed changes of barrier beaches to storm conditions, finding berm formation and barrier face erosion were controlled by wave climate, whereas crest lowering, overtopping and breaching were strongly linked to sea level.
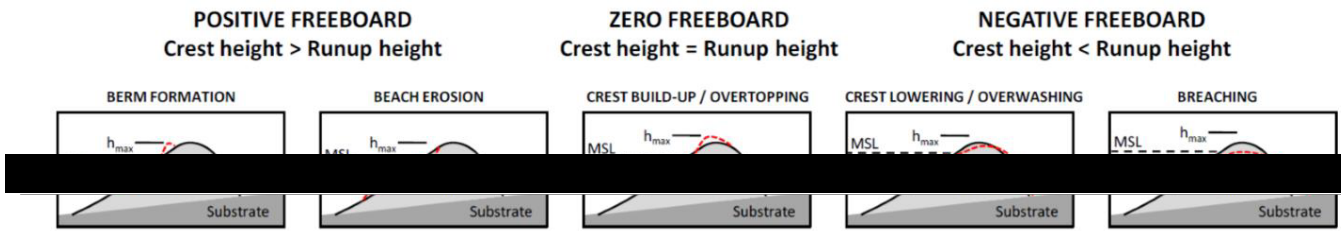
Figure 1.3- Conceptual model over barrier beach responses (McCall et al., 2015).

2.3.2 Empirical Models

Barrier beaches are natural form of coastal defence from extreme, adverse weather conditions (Bradbury & Powell, 1993). Protecting low lying coastline from storm surges and increasing frequency of storms. However, gravel beaches have been neglected in research when compared to the significant research and development of models for predicting the responses of sandy beaches. There has recently been interest in the modelling and analysis of gravel beach processes through physical and computational studies (McCall et al., 2013;Williams et al., 2012;Matias et al.,2014;Almeida et al., 2017;Masselink et al., 2010). Through this literature review an in-depth study into existing attempts to model and predict morphological changes to nearshore coastline enabled the development of the scope of this paper.

Wright & Short (1984) made an attempt to observe and collect data from beach profiles over a three-year period in 1979-1982 around the coastline of Australia. They found large variation in hydrodynamic conditions depending on the section of coastline. They created a conceptual chart relating the morphodynamic response to relative energy. Powell (1990) developed an empirical model for profile change on gravel beaches in the UK. He carried out a number of physical studies in a wave flume, varying conditions of both grain size and wave forcing conditions, validating the data against field data. Through this study a predictive framework was developed for the wave run-up, wave reflection coefficients and post storm beach profile. The work carried out by Powell (1990) was later developed in the SHINGLE model, using the still water level (SWL) as reference datum, three curves obtained through regression of the data gives the cross section of the beach profile predicting the height of the beach crest, the depth of the beach toe, and the location of both. Refer to Powell (1990) for full list of equations. Three non-dimensionalised parameters are developed, these are:

$$\frac{Hs}{D50} \qquad (1.12)$$

$$\frac{Hs}{Lm} \qquad (1.13)$$

$$\frac{HsTmg^{0.5}}{D50^{\frac{3}{2}}} \qquad (1.14)$$

The results of the paper are numerous, but the main conclusions of importance to this study were beach profile response is governed by wave height, wave period, wave duration, sediment diameter and angle of wave attack. It noted that within 500 waves 80% of volume change was likely to occur, and that initial profile does not affect the final form of the profile.

However, the experiments are limited to conditions that were used in the wave flume, as well as using normally forced wave conditions as well as the model assuming unlimited sediment budget. There was also limited beach profiles matching available hydrodynamic data, limiting the comparison to field data.
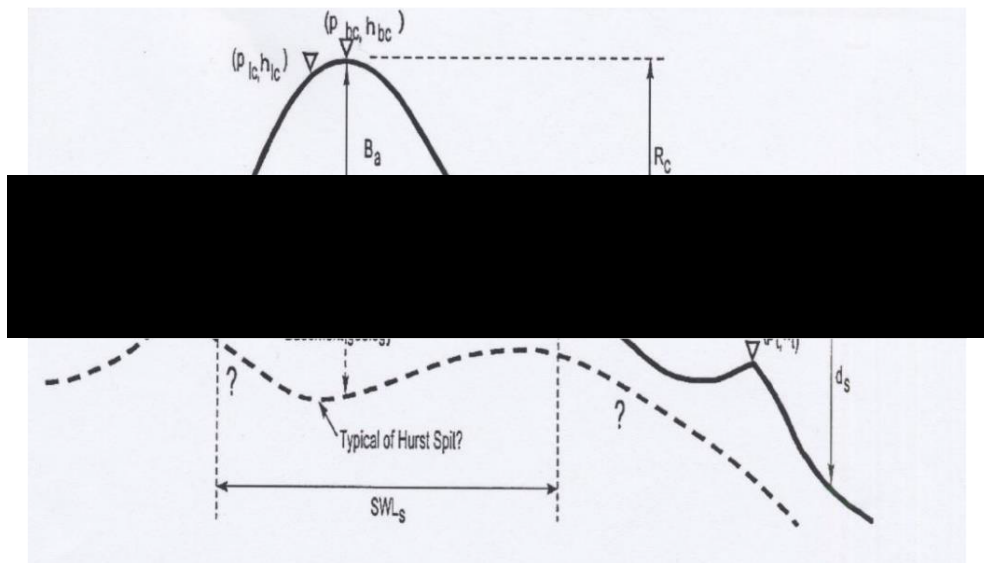
Figure 1.4 – Powell parametric model description of Hurst Spit from Powell (1990).

Bradbury built on the research of Nicholls (1985) and Powell (1990), through 3D physical modelling of the barrier beach Hurst spit. Through this he developed an estimate of barrier crest accumulation, overtopping and crest lowering processes. The study highlighted the importance of freeboard, especially between crest build up or crest lowering occurring through the overwash regime. The critical free board Parameter, C_f, offered some form of boundary for crest lowering or crest lowering to return, however $0.7 < C_f < 0.1$ crest lowering, or crest increase were possible. Bradbury identified that more data was required, however field measurements were limited.

Sallenger (2000) established a more comprehensive empirical model for barrier beaches by coupling the barrier geometry and the hydrodynamics which had largely been overlooked in previous studies. Four impact regimes were derived, relating the runup height to the barrier freeboard.:

- Impact 1-swash regime, wave run up is confined to the foreshore where there is no net change to barrier.
- Impact 2-collison regime, runup exceeds base of dune resulting in net erosion.
- Impact 3-overwash regime, the wave runup exceeds the barrier freeboard, resulting in net landward migration.
- Impact 4-Inundation regime, the storm surge is larger than the barrier freeboard continuously submerging the barrier.

Sallenger (2000) noted that the framework would use existing barrier geometry. However during a storm, the barrier geometry is ever changing as a result of the wave attack on the barrier and as a result the impact regime would also continually change.

Sallenger's model was later further developed by Donnelly (2007), through the analysis of 50 data sets through which Donnelly proposed seven barrier responses to storm conditions. They expanded on the four impact regimes set out by Sallenger (2000). Donnelly suggested the most important parameters to predict barrier response were extreme sea level, run-up level, overtopping duration, freeboard and dune volume. The extreme sea level had stronger correlation to overwash events than wave height, due to the decreased barrier freeboard, which agrees with Sallenger (2000) findings. Donnelly created a parametric flowchart to predict the response of barriers.

Bradbury (2000) and Bradbury et al., (2005) through multiple studies developed the Barrier Inertia Model, BIM. The model was an empirical threshold limit to predict, using initial barrier geometry and wave steepness, whether overwashing would occur on gravel barriers creating the barrier inertia parameter:

$$Bi = \frac{RcBa}{Hs^3} \qquad (1.15)$$

where Rc is crest height above SWL, Ba is the emergent cross section above SWL and Hs is the significant wave height. Originally derived through conditions taken from Hurst Spit, Bradbury calculated whether overwashing was likely to occur during storms of given return periods at Hurst Spit (Bradbury et al., 2005). The study found overwash likely to occur when:

$$Ib > 0.0006 \left(\frac{Hs}{Lm}\right)^{-2.5375} \qquad (1.16)$$

The study provided an accurate empirical model still used for shingle beaches today, however Bradbury (2000) proposed model is limited to the range of data used from Hurst Spit, where the model

is not valid for *Hs*/*Lm*<0.032. Although later validated for further cross sections and wave steepness range (Bradbury et al.,2005), Bradbury acknowledged that the model potentially underpredicted bimodal conditions (McCall et al., 2012).

Through a large scale physical experiment, the BARDEX experiment, which has been the centre of many studies (Matias, 2012; Williams et al., 2012; Turner & Masselink, 2012; Matias et al., 2014) present a large scale experimental study (BARDEX) on gravel beach dynamics. This was the largest, controlled study on gravel processes, looking at factors such as sediment properties, geology, and wave climate. Matias defined the overwash potential, OP, defined as the difference between the wave run-up and barrier crest elevation. Comparing the OP to 12 other run-up equations, the OP was found to be the most accurate. Due to the difference in Laboratory and Field conditions there is a small error of $\pm0.2m$ for OP>0.5m.

2.3.3 Process-Based Modelling

Although empirical models offer easy to use predictions for beach responses, they are often limited to the data available, field conditions and limited validations. Process based models capture the complex hydrodynamic and Morphological physical processes. The development of XBeach (Roelvink, 2009;Smit et al., 2010) and XBeach-G (Jamal, 2014; McCall et al., 2012, 2014, 2015) lead to wide ranging studies on gravel beaches and barriers. The physically processes behind XBeach can be seen in further detail in section 3.

Williams et al. (2012) used an early development of XBeach, not yet including the amendments made for gravel beaches, to compare the results to the BARDEX experiment, finding the model accurately reproduced the results of erosion with accuracy BSS of 0.6, however the model under predicted the location and size of the storm berm.

McCall et al. (2014,2015) and Masselink et al. (2014) presented their development of XBeach-G, which featured gravel sediment specific hydrodynamic and morphodynamics, to predict the l response of gravel beaches to storm conditions. The model showed differences in predicted overwashing events when compared to the barrier inertia model (BIM). Masselink et al. (2014) highlights the importance of Bimodal wave spectrum on increased overwash events, which is further supported by Orimoloye et al. 2019 and Thompson et al. 2018. Several other papers have used XBeach-G to simulate, with large success, the processes of gravel beaches and barriers.(Jamal et al., 2014; Williams et al, 2015;Poate, 2016;Bergillos, 2016;Almeida, 2017;Bergillos, 2017, Brown et al., 2019).

Williams et al. (2015) took the XBeach model and built an empirical framework to model the response of high energy coastlines to storm events. Using XBeach and field data to calibrate the model, Williams

et al. (2015) modelled the response of Rossbeigh Spit. The paper demonstrates that XBeach can effectively model the breaching and overwash of barrier island with 70% of BSS scoring good to excellent (0.6-0.8). Using Sallenger (2000) impact regime, site specific expressions were derived linking wave height, Hs, Storm surge and storm duration to corresponding impact regime. However, no physical meaning could be attached to the equation, limiting its usefulness. Williams et al. (2015) suggest that bottom friction and depth of wave breaking are important factors.

Another comprehensive study, using XBeach to derive an empirical expression for the overwash and runup on gravel beach was carried out by Poate et al. (2016). Poate used video derived runup statistics at six field sites across the south west English coast. These were coupled with an extensive number of XBeach models. Plotting the relative run-up $R_{2\%}$ was plotted against the Iribarren number:

$$\varepsilon_0 = tan\beta / \sqrt{\frac{H_0}{\lambda_0}} \qquad (1.17)$$

where

$$\lambda_0 = \frac{gT^2}{2\pi} \qquad (1.18)$$

T, is wave period, g is acceleration due to gravity, H_0 is deep water wave height and $tan\beta$ is beach slope. The new run up prediction has r^2 values of 0.97 and 0.89, which are categorised as very high predictions, with a wide-ranging use. The paper demonstrated the use of coupling field and synthetic data to provide the largest dataset to date for run-up data. Using synthetic data paired with field data has also been used to good effect by Almeida (2017), through which Almeida found that spectral shape of wave forcing conditions has a key role in morphological response of gravel barriers. Almeida found that bimodal wave conditions result in higher wave run up, due to longer wave period dominating the swash zone, resulting in increased chance overwashing event occurring.

3. Study site

3.1 Hurst Spit Castle

The Primary location of study throughout this study is HCS, a gravel barrier beach system forms the Christchurch Bay and provides protection from wave attack to an extensive area of low-lying land in the Western Solent in the south coast of the UK (Bradbury & Powell, 1992; Nicholls & Webber, 1989) (Fig. 3.1 and 3.2).
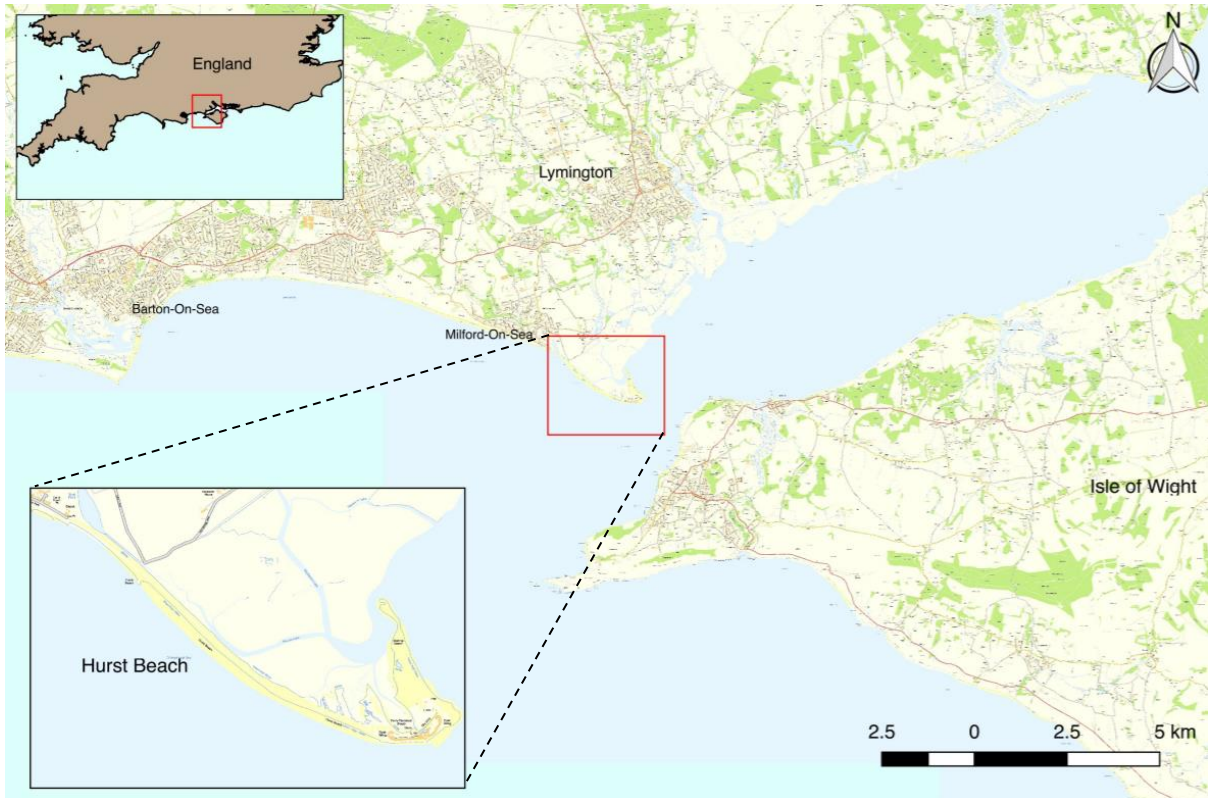
Figure 3.1- Location of primary Study, Hurst Spit Beach SW England located in the English Channel, UK.

The Spit is composed largely of shingle and is approximately 2.5 km long, orientated 130° North. The beach foreshore has an average slope of 8^0, with crest height varying significantly along the beach, ranging from 7m-3m ODN, from East to West.

The tidal range around the HCP is 2.2m where the spit is subjected to a meso-tidal regime. The predominant wave incidence is from the SSW. The Offshore bathymetry is complex. A shingle bank is located offshore of the HCP, which is exposed at low tide (Bradbury, 2003). There is also the North Heads bank running parallel to the shoreline. The banks have a sheltering effect on the spit from on-coming wave attack (Fig. 3.3).

HCS is a part of three international nature conservation designations, meaning it of considerable environmental and geological interest in developing an understanding of coastal geomorphology. There have been numerous overwash and breaching events over the past 200 years, prior to the implementation of a management plan for the spit in 1996-1997. The spit underwent a major recharge in 1996 as part of a 50-year shoreline management plan. Despite having an artificial beach crest following beach recharge, the spit is till prone to severe damage from storms, most recently seen in the February 2020 and in much greater effect during the 2013/2014 winter storms.

Figure 3.2- HCS aerial photograph, showing salt marshes and HCS located at the end of the spit (https://www.channelcoast.org)
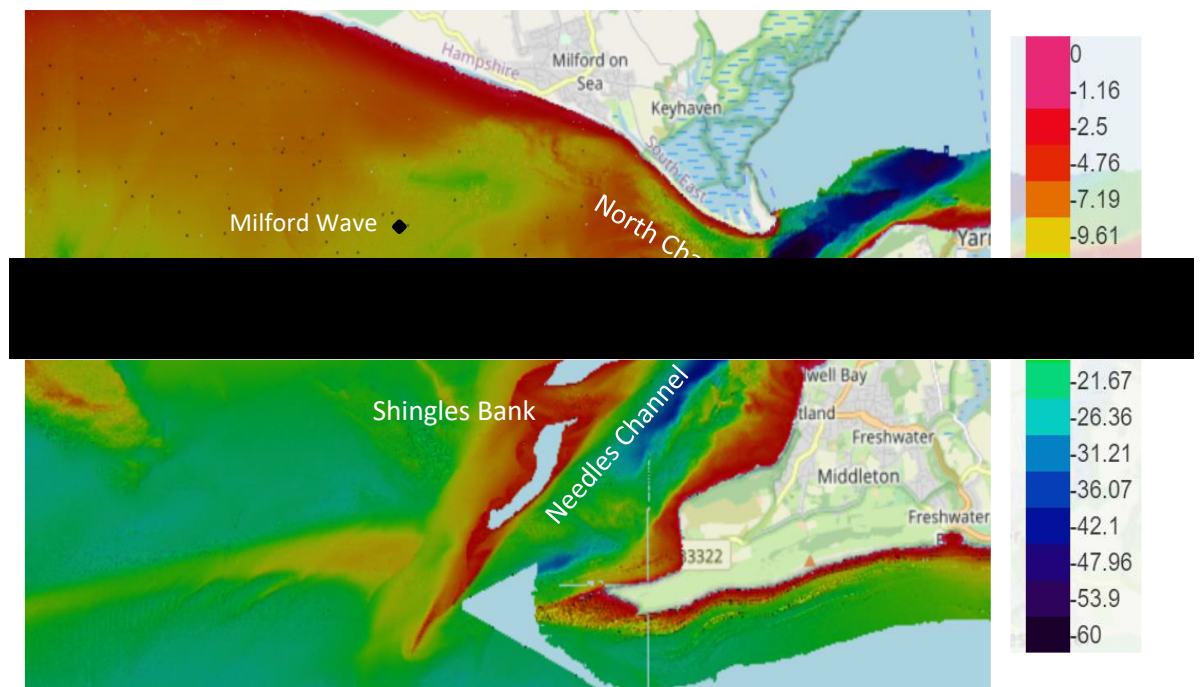
Figure 3.3 – Nearshore bathymetry of HCS gravel barrier beach and the surroundings. Bathymetry data are from https://www.channelcoast.org.

A wave buoy situated to the east of the HCS, at a water depth of 10m-12m mODN (Bradbury, 2000) which can be seen in Figure 3.3. Using the historical wave buoy data from the last 20 years (https://www.channelcoast.org) the annual average significant wave height (H_s), average peak wave period (T_p) and average wave direction have been determined to be 0.65m, 8.2s and 211° respectively. Through nearshore wave modelling and studying previous literature, Bradbury and Kidd (1998) found that the maximum significant wave height varies between 3.57m (240°) and 2.89m (210°) annually on the eastern end of the spit (Strete Gate) and between 2.10m (210°) and 2.68m (240°) at the western end of the spit (Torcross). Bradbury (1998) suggests that mean value of the maximum nearshore wave height declines along spit from the east to the west due to the attenuating or dissipating influence of the shingles bank and the North Bank, resulting complex wave refraction and wave train "crossover". Wave shoaling and breaking (at low water) induced by the complex bathymetry of the banks and channels seawards of the spit reduces the height of offshore waves by almost one third (Bradbury and Kidd 1998). The spit is highly vulnerable to high energy swell waves travelling across the Atlantic Ocean (Nicholls & Webber, 1989). When these swell conditions combine with mean high water springs and storm surges, the chance of overwash is found to be significantly increased (Williams et al., 2015).

HCS mostly shingle composition, with sediment diameter varying between 6mm-45mm, with the mean sediment diameter D_{50} of 15mm and D_{90} of 45 mm (Bradbury and Kidd, 1998; Bradbury & Powell, 1992). It is estimated that the main body of the HCS is declining in volume by approximately 7000-8000 m³/yr and retreating by 3.5m/yr on average (Nicholls & Webber, 1989). The littoral transport rate in the nearshore region has been estimated at 11,000-13,000 m³ per/yr (Nicholls, 1985). Littoral transport results in accumulation of sediment on the eastern tip of the spit, towards Hurst Castle (Nicholls, 1985).

The south-west of the UK is also subjected to frequent storms with bimodal characteristics as a result of swell-dominated waves reaching from The Atlantic Ocean (Thompson et al., 2018; Bradbury, 2011). Bradbury et al. (2007) found that bimodal conditions occur 25% of time during winter months where storms are frequent and severe, with the 0.25:1 year storm threshold of 2.74m. Nicholls and Webber (1989), Thompson et al. (2018) and some others reveal that bimodal storms may induce greater beach erosion and damage than their unimodal counterparts at certain occasions.

3.2 History of Hurst Castle Spit

HCS was originally formed from lose shingle from surrounding cliff faces of Christchurch Bay (Nicholls, 1985). Since the shoreline management plan implemented by the New Forest district council to Christchurch Bay region, in the early 1940s, sediment supply and therefore sediment at Hurst Spit has been in decline due to decreased littoral drift (Nicholls, 1985). There have been several notable storm events at Hurst, in 1962, 1981 (Nicholls and Webster, 1989) and 1989 (Bradbury 2000), which caused severe overtopping and overwashing. The 1989 storm had a 1:100 occurrence causing up to 80m rollback. Due to the barriers increasing rate of regression landward, the New Forest district council implemented a large scale beach management plan in 1996-1997.This increased the barrier width by up 20m and also increased the crest height up to 7m. Most recently the barrier was breached during the 2013/2014 winter storms (Bradbury & Mason 2014),where significant wave height exceeding 4.1m were recorded at Milford wave buoy, with storms in February 2014 having a return period of 1 in 50 years. Not only were individual storms large, but the sequencing of storms reeked particular havoc on the barrier, with 7 of the largest storms in last 10 years occurring during this time period (Bradbury & Mason 2014). The results of the 2014 storms can be seen in Figure 3.4. The Spit was restored after the 2014 events, however not to levels of the 1997 recharge.
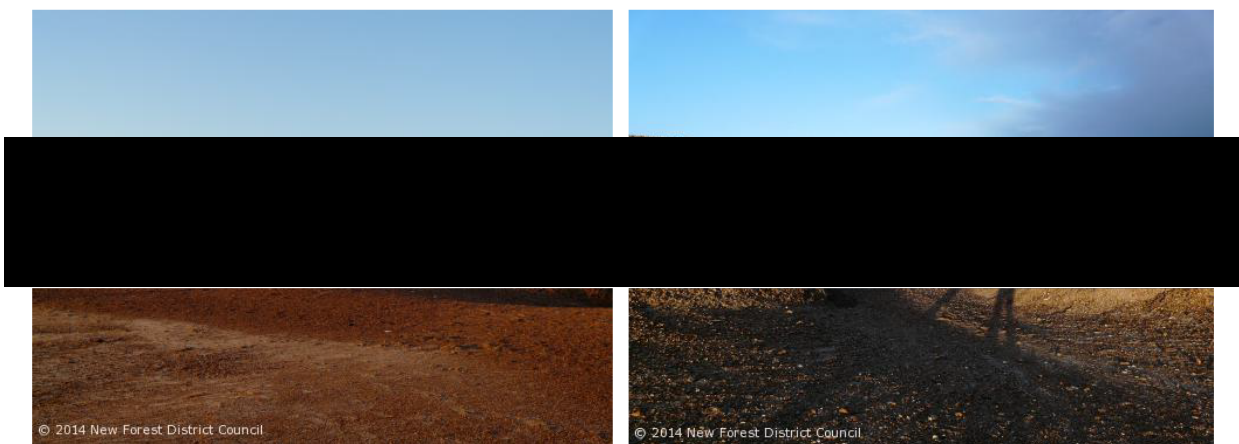
Figure 3.4- Photographs shows breaching that occurred at HCS during 2014 winter storms, some sections of the barrier are visibly lost completely with the saltmarshes behind the spit fully exposed (https://www.channelcoast.org).

3.3 Slapton Sands Beach

The secondary site used for validation, as seen in Figure 3.5 is Slapton Sands Barrier Beach, referred to as SSBB here after. SSBB is located similarly to HCS in the SW of the United Kingdom in the English Channel. SSBB experiences similar unimodal and bimodal wave conditions from the Atlantic Ocean

(Thompson et al., 2018). SSBB forms a part of Start Bay on the coastline of south Devon, UK, the barrier consists of shingle sediment, ranging from 1mm to 20mm in diameter (Chadwick et al., 2005). The barrier is 5km long and varies between 100m at low tide and 140m in width at high tide, with a tidal range of 2m at neap tide and 5m during spring tides. The barrier has an average crest height of 3.7m above MHWS separating the sea from a freshwater lagoon. Along the top of the barrier runs a main road, the A374, which has been severely damaged by past storm events, such as the 2002 winter storms which caused damage to a 250m section of the A374 (Chadwick et al., 2005).

Figure 3.5 - Location of secondary Study, SSBB, SW England located in the English Channel, UK.

4. Research Methodology

The scope of this thesis is to investigate the effects extreme conditions on barrier beaches, and to develop a simple parametric model to estimate gravel barrier morphodynamic response using Hurst Spit, UK as the study site. The extreme conditions in this study were defined as storm conditions occuring over the 0.25:1 year return period of 2.74m as defined by CCO .The thesis will look to take advantage of recent process based modelling to create a large synthetic dataset of varying storm conditions, enabling an empirical prediction model to be created-similar to the highly successful Barrier Inertia Model (Bradbury, 2000) and other similar models such as Donnelly (2007) and Stockdon et al. (2006). The model will build on Bradbury (2000) BIM model but will overcome some limitations of the model. Similar to Poate et al. (2016) where field measurements were combined with numerical model runs creating a large dataset of wave overwash and barrier volume change, enabling the development of the parametric model. The wave conditions in the model were forced via JONSWAP spectrum, the unimodal and bimodal inputs can be seen in section 5.1.

4.1 XBeach Model

The open source, process-based XBeach model was developed by Roelvink et al. (2009) as a sandy beach-dune erosion model. XBeach was originally developed as a short wave-averaged wave group resolving model and allowed short-wave variations in the wave group scale. The model resolved depth-averaged non-linear shallow water equation and the short-wave motion is solved using the wave action balance equation using the HISWA equation (Holthisijen et al., 1989).

XBeach offers three types of wave hydrodynamic forcing conditions. They include; stationary mode, solving wave averaged equations but neglecting infragravity waves; Surfbeat mode where short and long wave envelopes are resolved; lastly, the mode used throughout this study, Non-hydrostatic mode. Non-Hydrostatic calculations use depth average non-linear shallow water equations (NLSWE), including a non-hydrostatic pressure term and term for ground water exchange.

Later, the XBeach model was extended to include a non-hydrostatic pressure correction (Smith, 2010, 2013) to the depth-averaged non-linear shallow water equation which allows modelling of the instantaneous water surface elevation. The depth-averaged dynamic pressure is derived using a method similar to a one-layer version of the SWASH model (Zijlema et al., 2011). The non-hydrostatic XBeach model (named XBeachX) includes provisions for applications to gravel beaches (McCall et al., 2014, 2015). It also has a ground water model that allows infiltration-exfiltration through the

permeable gravel bed, which is a key process contributing to gravel beach morphodynamics and, gravel transport formulation of Van Rijn (2007) and numerous other sediment transport formulations (e.g. Soulsby, 1997; Van Rijn, 1993).The main advantages of using non-hydro static mode are that the short wave runup and overwashing are including in the model, this enables the model to capture with a high degree of accuracy the overwashing over beaches - which is of particular importance in gravel beaches and barriers. Another advantage is wave asymmetry and skewness are resolved in the model, reducing calibration required. The model captures wave breaking as well when waves exceed certain steepness the non-hydrostatic mode is disabled and replaced with momentum conserving shallow water equations (Smit et al., 2010). Smith further developed the non-hydrostatic model, to capture the breaking wave effects in plunging wave breaker, where bores form at $\frac{\partial \zeta}{\partial t} > 0.6$ and reform when $\frac{\partial \zeta}{\partial t} < 0.3$.

4.1.1 Model Governing Equations

The hydrodynamics of 1D XBeach non-hydrostatic model solves following equations:

$$\frac{\partial \eta}{\partial t} + \frac{\partial hu}{\partial x} = 0 \qquad (4.1)$$

$$\frac{\partial u}{\partial t} + u\frac{\partial u}{\partial x} - \frac{\partial}{\partial x}\left(v_h \frac{\partial u}{\partial x}\right) = -\frac{1}{\rho}\frac{\partial(\rho p_{nh} + \rho g\eta)}{\partial x} - \frac{\tau_b}{h} \qquad (4.2)$$

Where t is time, η is the water surface elevation from the still water level, u is the depth averaged cross-shore velocity, h is the total water depth, v_h is the horizontal viscosity, ρ is the density of seawater, p_{nh} is the depth averaged dynamic pressure normalised by the density, g is the gravitational acceleration and τ_b is the total bed shear stress given by

$$\tau_b = \rho c_f u|u| \qquad (4.3)$$

in which c_f is the dimensionless friction coefficient.

Where the horizontal viscosity v, which accounts for the absence of longshore current, is given as:

$$v = 2(c_s \Delta x)^2 \sqrt{2(\frac{\delta u}{\delta x})^2} \qquad (4.4)$$

c_s is the Smagorinsky constant, 0.1, and Δx is computational grid size. The depth averaged normalised dynamic pressure q is calculated from the mean dynamic pressure between the surface level, assuming pressure is zero is there, and the bed level:

$$\frac{\partial w}{\partial t} + \frac{\partial q}{\partial z} = 0 \qquad (4.5)$$

where wc is vertical velocity and z is the vertical coordinate.

Vertical velocity at the bed level assumes the kinematic boundary condition:

$$w_b = u\frac{\delta\xi}{\delta x} \qquad (4.6)$$

where ξ is bed level elevation.

$$\xi = \zeta - h \qquad (4.7)$$

Combining equation (4.6) and Keller Box method, the vertical momentum balance at the surface is given by:

$$\frac{\delta w_s}{\delta t} = 2\frac{q_b}{h} - \frac{\delta w_b}{\delta t} \qquad (4.8)$$

then by combining local continuity equation and equation (4.8):

$$\frac{\delta u}{\delta x} + \frac{w_s - w_b}{h} = 0 \qquad (4.9)$$

4.1.2 Ground Water Dynamics

Groundwater flow through, porous gravel beaches, is of significant importance in the post storm morphology (Li, 1997). The ground water model in XBeach assumes an incompressible, homogenous and Newtonian flow. The model computes depth averaged groundwater flows, as well as groundwater level and head fluctuations. Infiltration and exfiltration are also captured over unsaturated beds. Submarine exchange takes place in saturated beaches and exfiltration occurs in unsaturated material.

Horizontal groundwater flow in the aquifer is calculated using Darcy Law:

$$\frac{\delta h_{gw} U_{gw}}{\delta x} - W_{gw,s} = 0 \qquad (4.10)$$

$$U_{gw} = -K\frac{\delta\bar{H}}{\delta x} \qquad (4.11)$$

where U_{gw} is depth averaged horizontal groundwater velocity, $W_{gw,s}$ is the vertical groundwater velocity at the surface of ground water, h_{gw} is height of groundwater head above bottom of aquifer, $\bar{H}$

is depth averaged hydraulic head. In the case of the model the aquifer is assumed to be impermeable. Turbulent groundwater flow conditions are calculated by:

$$K = \begin{cases} K_{lam}\sqrt{\dfrac{Re_{crit}}{Re}} & Re > Re_{crit} \\ K_{lam} & Re \leq Re_{crit} \end{cases} \qquad (4.12)$$

where K_{lam} is laminar hydraulic conductivity, Re_{crit} is the critical Reynold number, to indicate the start of turbulent flow. The Reynolds number of ground water flow through a porous aquifer is

$$Re = \frac{|u_{gw}|D_{50}}{nv} \qquad (4.13)$$

where D_{50} is the median sediment diameter, v is the kinematic viscosity of water and n, is the porosity.

Through combination of vertical ground water head Eq. (4.14) and groundwater column Eq. (4.15) the depth averaged vertical ground water head can be calculated :

$$H(\sigma) = \beta\left(\sigma^2 - h_{gw}^2\right) + H_{bc} \qquad (4.14)$$

$$\bar{H} = \frac{1}{h_{gw}}\int_0^{h_{gw}} H(\sigma)d\sigma = H_{bc} - \frac{2}{3}\beta h_{gw}^2 \qquad (4.15)$$

where H is groundwater head, σ is the vertical coordinate above aquifer, β is parabolic curvature, H_{bc} is head on groundwater surface.

3.1.3 Sediment transport and bed updating

Sediment mobility in XBeach is calculated using shields parameter (McCall et al., 2015):

$$\theta = \frac{\tau_b}{pg\Delta_i D_{50}} \qquad (4.16)$$

where Δ_i is relative effective weight of the sediment. τ_b is the bed shear stress;

$$\tau_b = c_f \rho \frac{u|u|}{h} + \rho c_i D_{50} \frac{\partial u}{\partial t} \qquad (4.17)$$

where, c_f is dimensionless friction factor, u is depth averaged cross shore velocity, h is water depth, c_i is inertia coefficient to be calibrated in model, D_{50} is mean sediment diameter, ρ is density of sediment.

To account for the effects bed slope has on sediment mobility, effective shields parameter is used:

$$\theta' = \theta cos\beta(1 \pm \frac{tan\beta}{tan\emptyset}) \qquad (4.18)$$

where β is the local angle of the bed, $\emptyset$ is the angle of repose, typically between 30º-40º in gravel.

For $\theta cos\beta(1 \pm \frac{tan\beta}{tan\emptyset})$ < 1, sediment is transported up the slope.

For $\theta cos\beta(1 \pm \frac{tan\beta}{tan\emptyset})$ > 1, downward sediment transport occurs.

The above is then used to calculate sediment transport using Van Rijn (2007) bed load transport equation, excluding silt sediment coefficients:

$$q_b = \gamma D_{50} D^{-0.3} \sqrt{\frac{\tau_b}{\rho}} \frac{(\theta'-\theta_{cr})}{\theta_{cr}} \frac{\tau_b}{|\tau_b|} \qquad (4.19)$$

q_b is the bed load transport rate (volumetric), γ is the Van Rijn calibration coefficient set at 0.5 (Van Rijn, 2007). D is non-dimensionalized grain size and θ_{cr} is critical shields parameter, initiating sediment transport.

Bed level change in is then calculated in the centre of each grid cell, using the Exner equation (Paola et al., 2005):

$$\frac{\partial \xi}{\partial t} + \frac{1}{(1-n)} \frac{\partial q_b}{\partial x} = 0 \qquad (4.20)$$

$\frac{\partial \xi}{\partial t}$ is the change in elevation of bed above datum over time and n is the porosity. Avalanching occurring is captured through comparison of bed level slope and angle of repose (Roelvink, 2009):

$$|tan\beta| > \emptyset \ avalanching$$
$$|tan\beta| \leq \emptyset \ no \ avalanching \ occuring$$

The reader is referred to McCall et al. (2014, 2015) and the XBeach Manual (https://xbeach.readthedocs.io/en/latest/xbeach_manual) for full details of the model.

4.2 XBeach model setup and calibration for Hurst Castle Spit

Prior to the application of the XBeachX model for gravel beaches to generate a synthetic series of gravel barrier overwash and profile evolution from extreme conditions at Hurst Castle Spit, hereafter referred to as HCS. The model was calibrated using field measurements at the HCS. A 1D model was established, for two cross sections (Fig. 4.1) of the barrier beach using measured pre-storm barrier cross-sections. The cross sections and hydrodynamic conditions were chosen from Bradbury et al. (2005) study where HS1 was identified as sufficient in size to experience no overwashing and HS2 was identified as vulnerable to overwash during a 1:5 year storm event (Bradbury et al., 2005).

Table 4.1 shows cross-sections and storm conditions used for model calibration. The selected cross-sections vary in size, shape and crest height and have different degrees of susceptibility to storm erosion. The model domain was extended until the 15 m water depth using a 1:50 beach slope, which is sufficiently steep to have no effect on waves at the model boundary in the subtidal region to ensure no wave transformation between Milford wave buoy and the model boundary. The offshore and nearshore bathymetry required for numerical model domain development were obtained from the bathymetry measurements of the Channel Coastal Observatory (CCO) of the UK (https://www.channelcoast.org). A 1D, non-equidistant grid system, oriented with the x-axis in the cross-shore direction along the cross-section, positive towards the shoreline, is used. The 1D grid is used to capture to cross-shore processes whilst neglecting the longshore processes that could be captured using a 2D grid. The grid cell size varied from 2m-3m offshore to 0.1m-0.3m onshore, which allowed the model to capture the complex morphodynamics of the beach cross section, whilst offshore grid sizes are sufficient in size to capture wave transformations occurring in the non-hydro static model.

The input storm wave boundary conditions were derived from the wave buoy data from the Milford wave buoy (50°42'.75N 001°36'.91W) located at 10 mODN water depth off the coast of Milford on sea. The wave buoy is located to the left side of the shingle bank and the North Head Bank (Fig. 4.3). The two storms vary considerably in their characteristics where one storm is dominated by long distance swell approaching from the Atlantic Ocean and show evidence of strong bimodal seas while the other one is dominated by local wind waves. Water levels during the storms were derived from the nearest tide gauge located in Christchurch Bay, from the UK tide Gauge Network (https://www.bodc.ac.uk/data/hosted_data_systems/sea_level/uk_tide_gauge_network/). Storms were determined based on the storm threshold wave height defined by the CCO for south-west region

of the UK where waves are considered as storm waves if the significant wave height exceeds the 0.25 yr return period significant wave height (https://www.channelcoast.org/realttimedata). Storm surge was derived from Coastal flood boundary conditions for UK mainland and islands (DEFRA 2018). It should be noted that the selection of storm conditions used for model calibration was limited by the availability of accurate pre- and post-storm beach profile measurements at HCS.
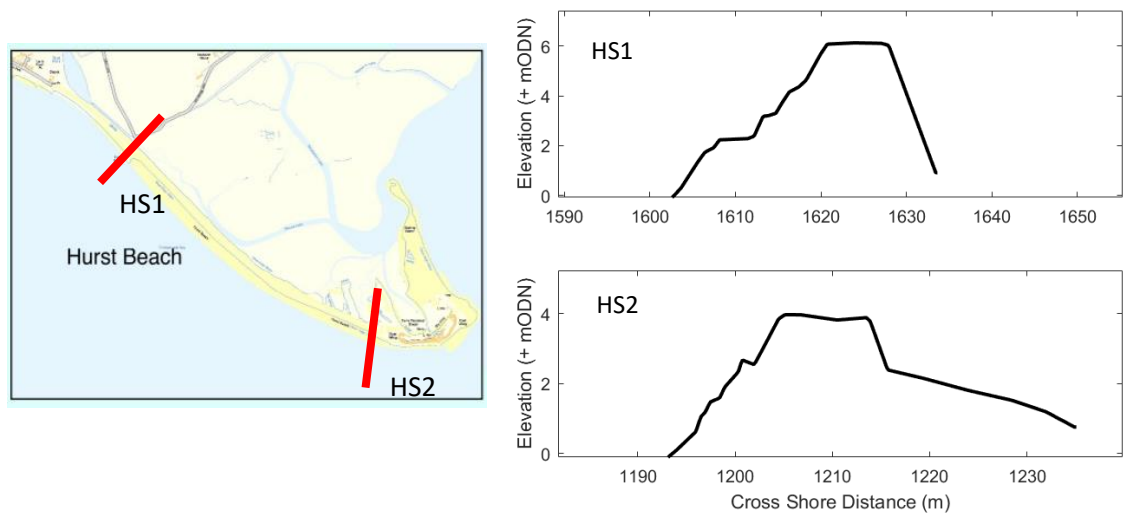
Figure 4.1 – Cross sections of the HCS gravel barrier beach used for model calibration and their locations. Locations (left) and cross section profiles (right).

Table 4.1 – HCS gravel barrier cross-sections and storm conditions extracted from the Milford wave buoy for model calibration, used for XBeach model validation. $(H_s)_{max}$ = maximum significant wave height; T_p = peak wave period from the JONSWAP spectrum; ϑ = wave approach direction from the north; MHWS = mean high water surface during the storm. S1 – storm 1, S2 – storm2.

Cross Section	Crest Height m ODN	Pre-Storm Profile Date	Post-Storm Profile Date	Storm duration (hrs)	$(H_s)_{max}$ (m)	T_p (s)	ϑ	Surface elevation above ODN(m)
HS1-S1	6.27	28/10/2011	31/10/2011	10 (S1)	2.75	18	220	1.1
HS1-S2	6.27	11/09/2011	13/09/2011	24 (S2)	3.85	8.3	216	0.928
HS2-S2	3.96	11/09/2011	13/09/2011	24 (S2)	3.85	8.3	216	0.928

Figure 4.2 shows a comparison of measured and XBeach-simulated post-storm cross-shore profile response of the HCS for storm conditions given in Table 4.1, following model calibration. The model

used gravel beach sediment transport formulation given in McCall and Van Rijn (2015) and used D_{50} of 15mm and D_{90} of 45 mm (Bradbury & Kidd 1998).

To accurately quantify the comparisons, the Briers Skill Score (BSS) (Van Rijn 2003) and RMSE are utilised. The BSS categorises the model's ability to correctly predict profile changes, where a score of 0-0.3 indicates 'poor' prediction, 0.3-0.6 indicates a 'reasonable/fair' model prediction, 0.6-0.8 indicates a 'good' score and lastly a score of 0.8-1.0 an excellent prediction.

$$BSS = 1 - \left[\frac{(X_m - X_p)\text{^}2}{(X_b - X_m)^2} \right]$$

Where X_m modelled post storm profile, X_p is measured post storm profile and X_b is measured pre storm profile.

Both the skill score and RMSE were calculated using the profile change above 0 mODN (Ordnance Datum Newlyn) due to the lack of accurate pre and post storm bathymetric measurements below 0 mODN. The primary calibration parameters and the final selected values are given in Table 4.2.
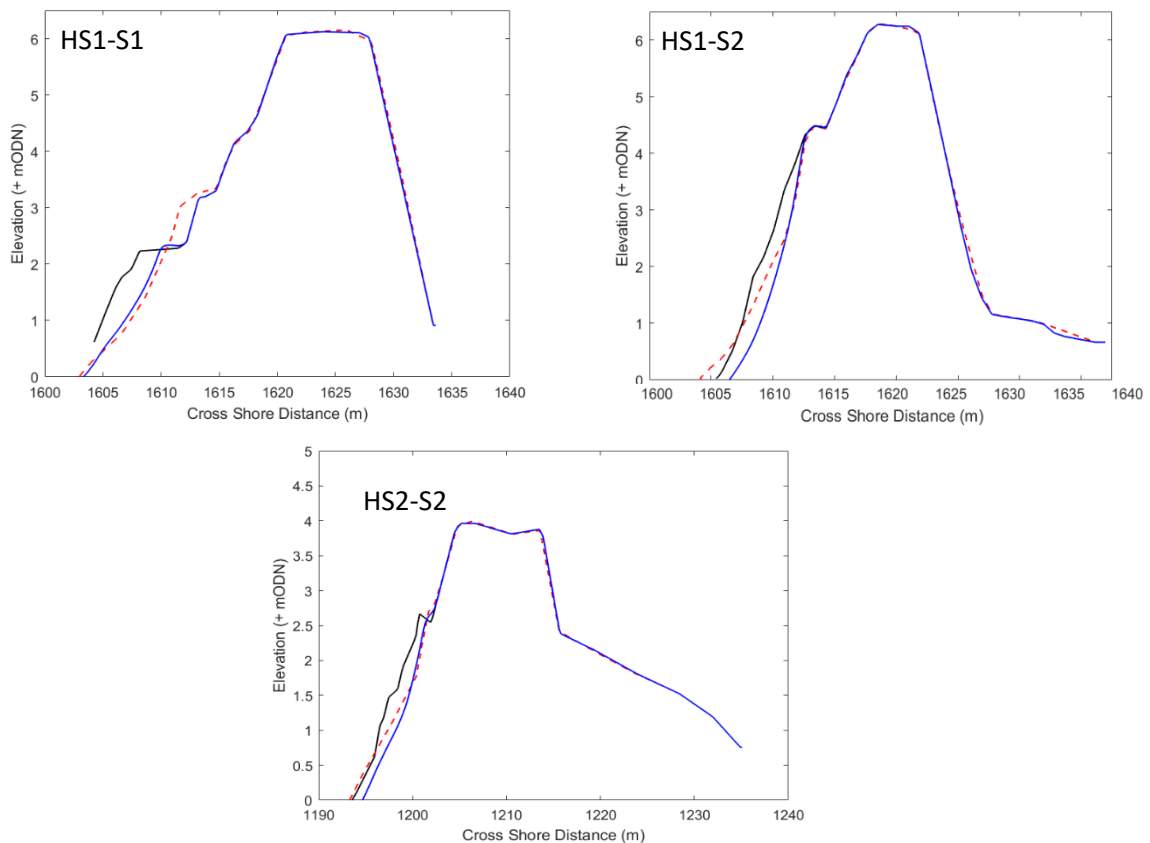
Figure 4.2 – A comparison of measured and simulated post-storm profiles (HS1-top and HS2-bottom) at HCS following XBeach model calibration against storms S1 and S2. Measured pre-storm profile (black line), measured post-storm profile (red dotted line) and simulated post-storm profile (blue line).

Table 4.2 – Calibration parameters of the XBeach non-hydrostatic model of the HCS gravel barrier beach.

Model parameter	*Recommended range*	*Default value*	Selected value
dryslp	0.1-2.0	1.0	1.0
wetslp	0.1-1.0	0.3	0.3
CFL	0.7-.9	0.7	0.9
reposeangle	0-45	30	45
kx	0.01-0.3	0.01	0.15
ci	0.5-1.5	1.0	1.0
morfac	1-1000	1	1
cf	3D90	3D90	3D90

Where *dryslp* is critical avalanching slope above water level, *wetslp* is critical avalanching slope below water level, *CFL* is maximum courant Friedrichs-Lewy number, *repose angle* is the angle of internal friction of sediment, *kx* is hydraulic gradient, *ci* is mass coefficient in shields inertia term, *morfac* is the morphological acceleration factor and *cf* is the bed friction factor.

The calibration results reveal that the model is capable of satisfactorily capturing the morphodynamic response of the HCS gravel barrier to storms. Profile change at HS1-S1 case scored BSS of 0.62 and RMSE 0.24. HS1-S2 scored BSS of 0.6 and RMSE of 0.14 while HS2-S2 scored BSS of 0.78 and RMSE of 0.094, providing either 'good' or 'excellent' predictions.

It should be noted that the model underpredicted the berm formation in HS1-S1, but the erosion of the lower beach is captured well. The model slightly overpredicted the erosion of the intertidal zone in HS1-S2 but upper beach, which is the most important areas in terms of barrier area change, is

correctly modelled. In HS2-S2, the accretion of sediment on the upper beach area is captured very well although there was some overprediction of profile erosion in the lower beach area.

4.3 XBeach model validation

Direct validation of the HCS model against barrier overwash was not possible due to lack of overwash data. Therefore, the model was used to simulate if overwash occur at HS1 and HS2, following Bradbury (2000), during a series of statistically significant synthetic storms given in Table 4.3.

Bradbury (2000) Barrier Inertia Model (BIM) given in Equation (4.21), states that if the barrier inertia parameter $\frac{R_c B_a}{H_s^3}$ is smaller than $0.0006 \left(\frac{H_s}{L_m}\right)^{-2.5375}$, overwashing will occur.

$$\frac{R_c B_a}{H_s^3} = 0.0006 \left(\frac{H_s}{L_m}\right)^{-2.5375} \quad \text{for} \quad 0.15 < \frac{H_s}{L_m} < 0.032 \qquad (4.21)$$

where R_c is barrier freeboard, B_a is barrier cross sectional area above static water level, H_s is the significant storm wave height and L_m is wavelength corresponding to mean wave period. Please refer to Figure 3.3 for definitions of variables.

Using Equation (4.1), Bradbury (2000) estimated HS1 will not overwash during any of the storms given in Table 3.3 while HS2 will overwash during all storms except 1:1 year storm.

Table 4.3 – Storm conditions used to model barrier overwash at HCS.

Storm Return Period	H_s (m)	T_m (s)	Surge imposed on MHWS ODN (m)
1:1	3.69	8.64	1.0
1:10	4.22	9.30	1.0
1:20	4.39	9.48	1.0
1:50	4.6	9.71	1.0
1:100	4.75	9.87	1.0
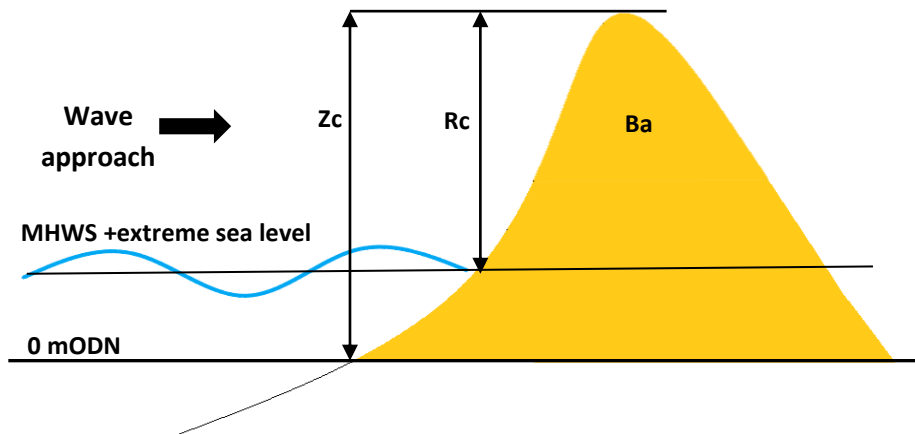
Figure 4.3– Schematisation of barrier geometry. B_a = pre-storm barrier cross sectional area above Extreme sea level mODN + MHWS, R_c = initial barrier freeboard and Z_c = initial barrier crest height

Figure 4.4 compares simulated barrier inertia with Bradbury et al. (2005) barrier inertia threshold at HS1 and HS2 from the 5 storm wave conditions given in Table 4.3. At HS1, only the most severe storm event, 1:100, resulted in small amount of wave overtopping. In contrast, all storm events other than the 1:1 storm resulted in some overwashing or overtopping at HS2. Both results are in good agreement with the BIM, as shown in Figure 4.4, highlighting that the HCS model correctly simulates if overwashing will occur during a storm. This result gives confidence in using the numerical HCS model for predicting overwashing volumes during storms.
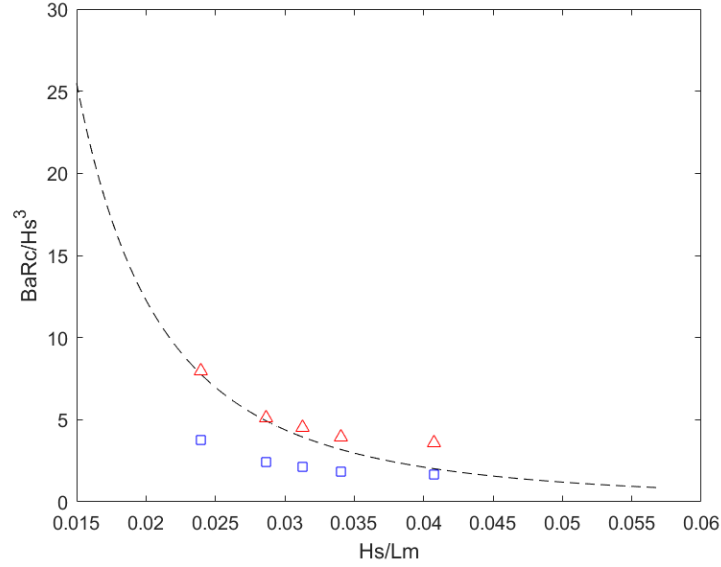
Figure 4.4 – Comparison of Bradbury (2000) Barrier Inertia Model and XBeach simulations. Black line – overwash threshold given by Barrier Inertia Model of Bradbury (2000). Red triangles and blue squares are XBeach simulations at HS1 to HS2, respectively.

4.4 Parametric model development

To develop an empirical model, numerically simulated barrier volume change and overwash data will be analysed through regression. The method of Least Squares Fitting was implemented for all regression models detailed in the following results section. The least squares method minimizes the summed square of the residuals:

$$r_i = y_i - \widehat{y_i} = y_i - b_0 - b_1 x_i \qquad (4.22)$$

Where r_i is the difference of observed and fitted values, y_i original data point, $\widehat{y_i}$ is the fitted data point. For Linear least square regression, the Sum of Square residuals is given below:

$$SS_{res} = \sum_{i=1}^{n} r_i^2 = \sum_{i=1}^{n} (y_i - \widehat{y_i}) \qquad (4.23)$$

$$b_1 = \frac{SS_{xy}}{SS_{xx}} \qquad (4.24)$$

$$b_0 = \bar{y} - b_1 \bar{x} \qquad (4.25)$$

Where SS_{res} is the sum of squared error estimate and n is the number of data points used in regression, $\bar{y}$ and $\bar{x}$ are sample means.

$$SS_{xx} = \sum_{i=1}^{n} [x_i - \bar{x}]^2 \qquad (4.26)$$

$$SS_{xy} = \sum_{i=1}^{n} [y_i - \bar{y}][X_i - \bar{X}] \qquad (4.27)$$

The assumption of normally distributed residuals must be true for use of prediction and confidence intervals.

For the formation of the regression curve, the MATLAB curve fitting toolbox was used. This uses iterative methods and the Levenberg-Marquardt algorithm (Levenberg, 1944) run via MATLAB to find the best fit. By optimizing parameter θ for function $f(x_i, \theta)$, the above least squared regression equation can be given by:

$$F(\theta) = \frac{1}{2} \sum_{i=1}^{n} r_i^2 \qquad (4.28)$$

The goodness of fit statistics to determine how well the regression model predicts dependent variables are described below:

Total Sum of Squares- $\qquad SS_{tot} = \sum_i (y_i - \bar{y})^2 \qquad (4.29)$

Regression Sum of Squares - $\qquad SS_{reg} = \sum_i (\hat{y}_i - \bar{y})^2 \qquad (4.30)$

Sum or Squared Residuals- $\qquad SS_{res} = \sum_i e_i^2 \qquad (4.31)$

Proportion of total variation in y that accounted for by regression line, ranging from 0-1, values closer to 1 indicate the model prediction accounts for more of the data points-

$$R^2 = 1 - \frac{SS_{reg}}{SS_{tot}} \qquad (4.32)$$

The R^2 is adjusted for the degrees of freedom:

$$MS_{tot} = \frac{\sum_i (y_i - \bar{y})^2}{n-1} \qquad (4.33)$$

$$MS_{res} = \frac{SS_{res}}{n-k} \qquad (4.34)$$

$$R^2_{adjusted} = 1 - \frac{MS_{res}}{MS_{tot}} \qquad (4.35)$$

Where n= number of observations and k is number of pairs of observation.

Confidence intervals provide a range that data should fall if experiments were repeated within the original range tested. It is denoted by $100(1 - \alpha)\%$, where α is defined bound, for 95% confidence limit $\alpha = 0.05$. Confidence bounds are given by:

$$\hat{y} = (x_0) \pm \left(t_{n-2,\alpha/2} \sqrt{MS_{res} \left(\frac{1}{n} + \frac{(x_0 - \bar{x})^2}{SS_{xx}} \right)} \right) \qquad (4.36)$$

4.5 Alternative modelling approaches

As previously discussed in Section 2.0 there are several other options to model beach profile change. The Powell (1990) model whilst useful for predicting beach face profile change under low-energetic storms has many limitations. The model cannot predict overwashing processes and assumes there is infinite sediment, resulting in very inaccurate results during large storms where overwashing occurs. The BIM model (Bradbury et al., 2005; Bradbury, 2000) is limited to only predicting if overwashing will occur and not quantifying the morphological changes to the barrier. XBeachX is the most advanced processed-based modelling approach developed to date which has been extensively validated as discussed in Section 2.0.

There are uncertainties with XBeach due to the extensive list of parameters to be calibrated. The uncertainties, however, are mainly dealt with thorough model validation and the use of multiple simulations under a range of different environmental scenarios. Parametric uncertainties are dealt with sensitivity analysis. A selection of a different process model will not give much different results as most available process models to date have very similar process description and a set of validation parameters. However, some very subtle differences between model numerical schemes and process descriptions there can be some very small deviations which may not be significant.

5. Modelling gravel beach profile change and overwash scenarios

5.1 Model set up

In order to develop a simple parametric model to estimate gravel barrier profile change of a wide variety of gravel barrier beaches under storm conditions, the calibrated XBeachX model was used to generate a large number of barrier response realisations. A range of barrier cross-sections and storm conditions were used. HS1 and HS2 were chosen, as were 3 other cross sections between them to encompass the range of barrier geometry in the model. Synthetic storm conditions were developed following a statistical analysis of long-term wave measurements of the Milford wave buoy. The waves have been measured since 1996 at 1Hz from which significant wave height, peak wave period and mean wave period have been calculated every 30 mins. Fifteen statistically significant storm wave heights and four peak wave periods with varying return periods between 1:1 and 1:100 years were calculated using the measured wave data from Bradbury et al. 2005 in which 19 years of wave buoy data had a Weibull distribution fitted. A JONSWAP spectrum was used to generate storm wave conditions. Storm duration was kept constant at the mean storm duration of 20 hours the average storm duration of the past 5 years - determined from the Milford wave data, taking the storm threshold wave height of 2.74 m as defined by CCO.

Six storm surge levels with return periods 1:1, 1:10, 1:20, 1:50, 1:100 and 1:200 (Figure 5.1), were selected from the coastal flood boundary conditions for UK mainland and islands report (DEFRA, 2018), taking values at 95% confidence values. Those were combined with tide data (Figure 5.2) to determine extreme total water levels. The storm surge shapes were derived using 5 years of historical tidal data and taking the average shape of the largest 15 surges over that time period and normalising the shape. This followed the method laid out in the DEFRA 2018 manual for flood boundary design conditions (DEFRA, 2018). The double peak observed in the tides in Southampton and Christchurch Bay is due to shallow water effects interacting with tidal harmonics. The tidal currents are known to have velocities that that are capable of transporting coarse sediment (Nicholls, 1980). It was assumed that the storm peak intensity and the maximum value of storm surge occurred at the highest tide in order to model the worst-case scenario for each numerical simulation. Five different barrier beach cross sections from HCS with varying shapes and crest elevations were selected, as seen in Figure 5.3. Figures 5.3 (A), (B),(C), were taken from topographic data from 3 different locations. Figure 5.3(A) was taken at the most northernly location (HS1) and Figure 5.3 (B) was the most southernly location. HS2 and Figure 5.3(C) and (E) were taken at some distance between the previous locations. Figures 5.3 (D) is a post storm profile, offering an insight into very vulnerable barrier cross sections.

The storm conditions, water levels and profile shapes were then combined to generate 880 realisations of physical plausibility of input conditions (Table 5.1) to drive the XBeach model to simulate profile change and overwash. 36 realisations of bimodal storm conditions with six different swell percentages were also generated using data in Table 5.1.
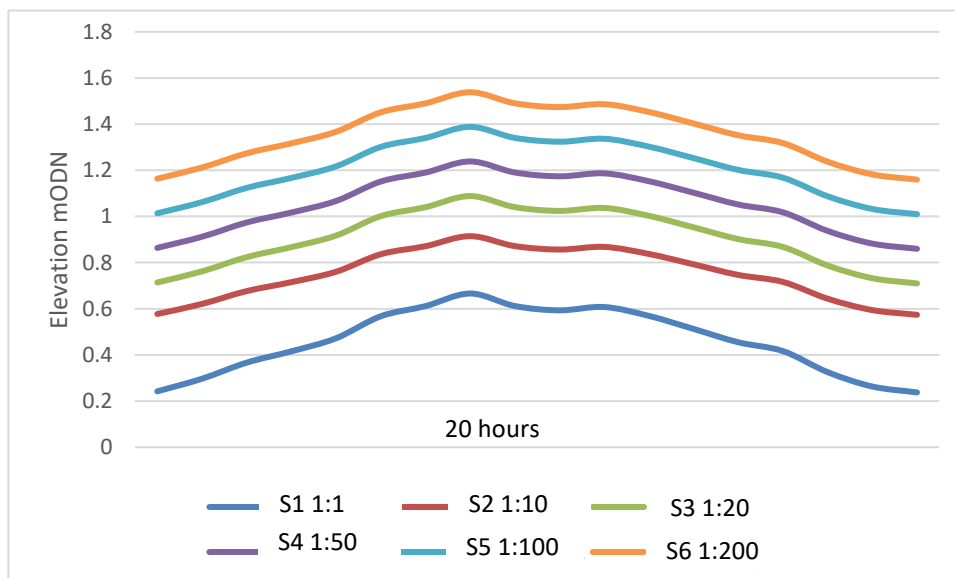
Figure 5.1- Extreme storm surges which were imposed on the MHWS seen in figure 5.2 and mean profile shape derived from DEFRA 2018. Legend displays surge reference (e.g. S1) and the corresponding return periods (e.g. 1:1)
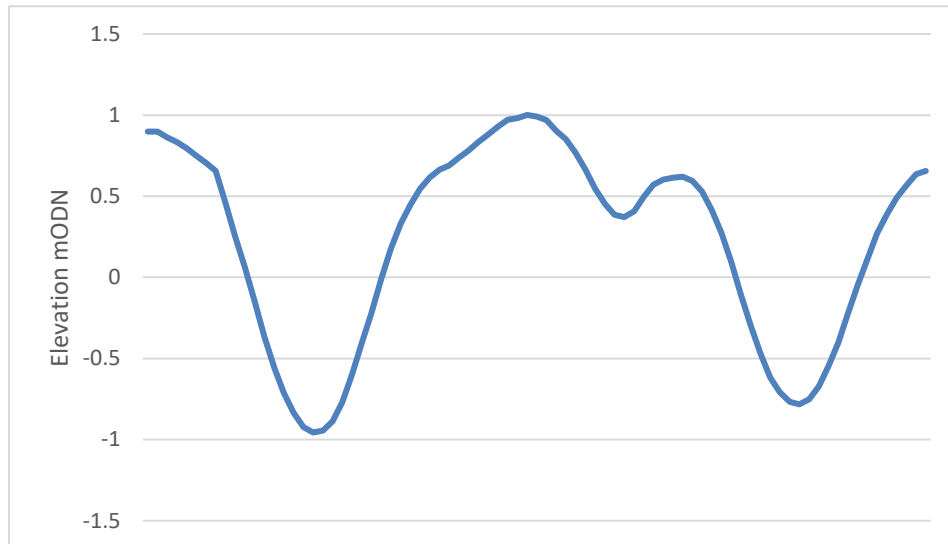
Figure 5.2- Mean High Water Spring Tidal elevation used for XBeachX simulations, data made available by (https://www.channelcoast.org) for Christchurch Bay tidal Gauge.

Table 5.1 – Example of a Unimodal JONSWAP input file. hm0 is Significant wave height (m), Tp is peak wave period (s), mainang is wave approach angle, gammajsp is JONSWAP peak enhacment factor, s is spreading coefficient and fynq is highest frequency used to create JONSWAP.

hm0	3.64
tp	8
mainang	215
gammajsp	3.3
s	14
fnyq	0.3

Table 5.2 – Example of Bimodal JONSWAP input file. Where nmodal=2 indicates bimodal spectrum, Hm0 is Significant wave height (m), fp is peak frequency, mainang is wave approach angle, gammajsp is JONSWAP peak enhancement factor and s is spreading coefficient.

nmodal	2	
hm0	2.05	3.56
fp	0.2	0.067
mainang	210	210
gammajsp	3.3	1
s	10	70

Table 5.3 – *Significant wave heights, peak periods and storm surges with a range of return periods used to generate synthetic unimodal and bimodal storm events.*

Unimodal cases			Bimodal cases		
H_s (m)	T_p (s)	MHWS+surge above ODN (m) (Extreme sea level ESL)	Hs (bimodal)(m)	MHWS+surge above ODN (m) (Extreme sea level ESL)	Swell percentage
2.75, 2.94, 3.13, 3.31, 3.50, 3.64, 3.76, 3.87, 3.99, 4.11, 4.22, 4.34, 4.46, 4.57, 4.69, 4.75	8.0, 9.0, 10.0, 11.5	1.52, 1.80, 1.96, 2.07, 2.20, 2.40	2.75, 3.64, 4.10, 4.75	1.52, 1.80, 1.96, 2.07, 2.20, 2.40	10, 25, 35, 40, 50, 75
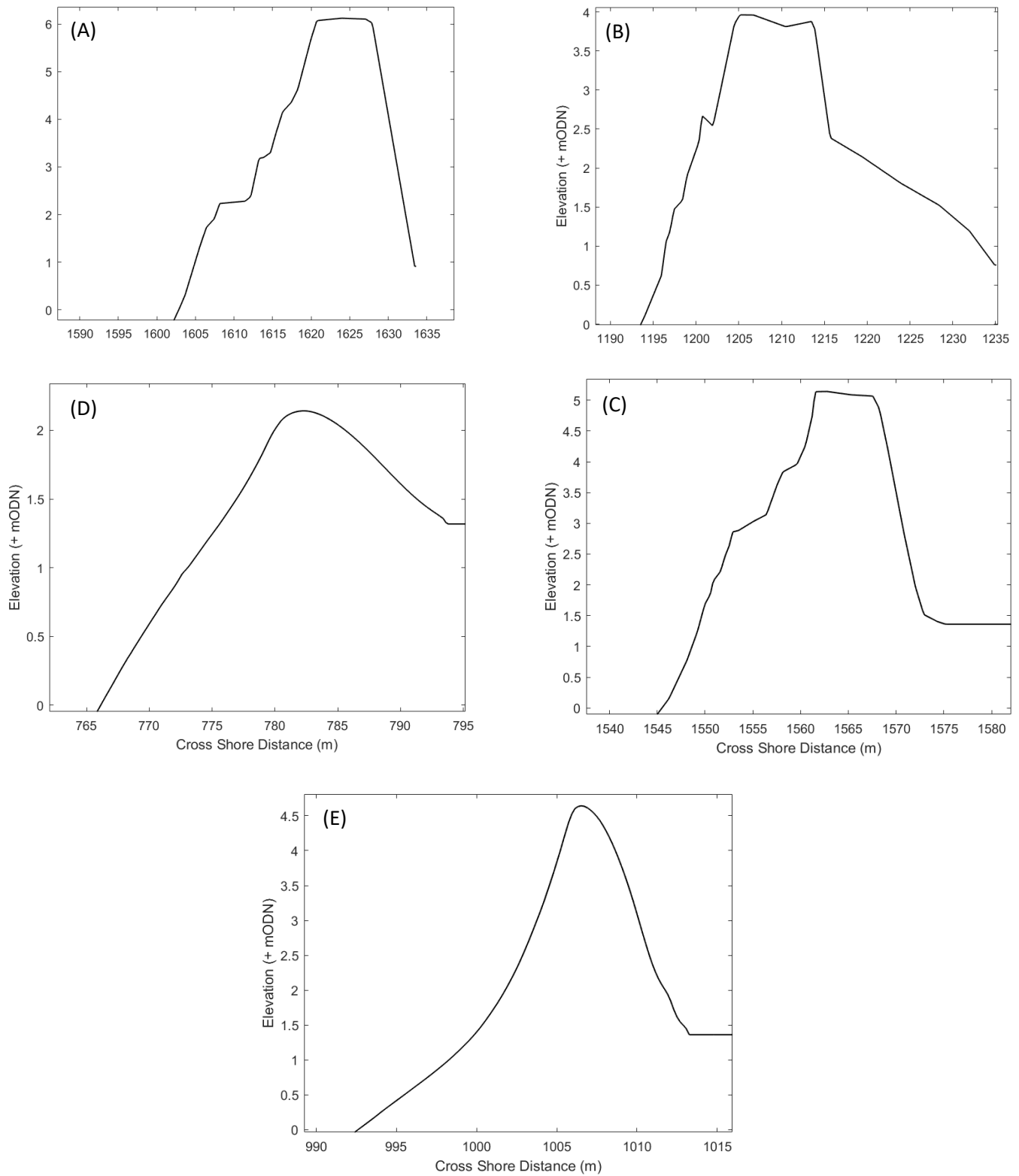
Figure 5.3- (A)- HS1 (Cross shore 1) profile, (B)- HS2 (Cross shore 2) profile (C)- HS3 (Cross shore 3 profile) (D) HS4 (Cross shore 4 profile) (E) HS5 (Cross shore 5 profile). Cross shore distance is 0m at the offshore boundary in XBeach model domain.

6. Results and Discussion

In this section results of numerical simulations and a detailed investigation of gravel barrier response to extreme conditions are presented and discussed.

6.1 Initial Observations

Figure 6.1 shows the impacts of varying a single parameter at a time on the morphodynamic change of HS2 profile. As the value of peak wave period, Tp, increases there is greater change to the barrier post storm profile. For smallest Tp value of 8s, HS2 barrier response is limited to only face erosion and some crest accumulation. Tp = 9s results in small amounts of overtopping/overwashing occurring with some sediment deposited on the crest of the barrier. There are some amounts of sediment deposited at the back of the barrier due to overtopping of waves. The same effects are also observed for Tp = 10s, albeit to a greater magnitude. Finally, Tp = 11.5s results in most significant profile change with the mode of barrier response changing entirely to crest lowering because of overwashing. The amount of offshore sediment transport is also decreasing as Tp increases. These observations highlight a several key assumptions. Firstly that as wave period increased, which leads to larger wave lengths, there is an increased run up, carrying more sediment up the beach face due to waves being able to propagate closer to shore without dissipation. This is seen clearly with increased amount of sediment deposited behind on the back of the barrier. Secondly it indicates wave period has strong enough influence on profile response to change the barriers mode of response.

Figure 6.1(B) highlights the effects wave height Hs has on post storm profile. It shows that all values of Hs have the same mode of response on the barrier, which is crest lowering as a result of overwash. As Hs increases, crest lowering increases, with increasing amount of sediment being deposited at the back of the barrier. As Hs increases there is a small increase in sediment transported offshore. This can be explained by more volume of water reaching the beach face in propagating wave, the beach becomes saturated quicker and there is greater backwash as new waves cannot percolate into the face, resulting in greater offshore transport (Polidoro et al., 2018). This observation is in good agreement with Austin & Buscombe (2008) and Austin & Masselink (2006) that increased wave height is responsible for larger amounts of offshore sediment transport due to increased cross-shore velocity, increasing bed shear stresses and entrainment forces.

Finally, Figure 6.1(C) shows the effect extreme sea level has on the post storm profile. The impacts of increased storm surge imposed on the tidal elevation (ESL) are twofold. Firstly they decrease the relative freeboard of the profile which increases the vulnerability to wave overtopping (Sallenger, 2000) and secondly decreases the area of the barrier which again makes the barrier less stable. The wave attack is also shifted closer to shore as waves can break closer to shore (Bradbury, 2000). The above reason explains why ESL induce a large variation of impacts on the barrier profile. The lowest ESL values of 1.52 mODN, a 1:1 year occurrence, result in relatively little impact, with some overtopping and crest accumulation observed. The mode of barrier response is then changed to crest lowering, for ESL of 1.80 m and 1.96 m, where the crest is lowered through overwashing. A similar response is observed for ESL of 2.07 m but to a greater magnitude, where the barrier is almost inundated. Inundation is observed for the two largest ESL where the barrier is breached.
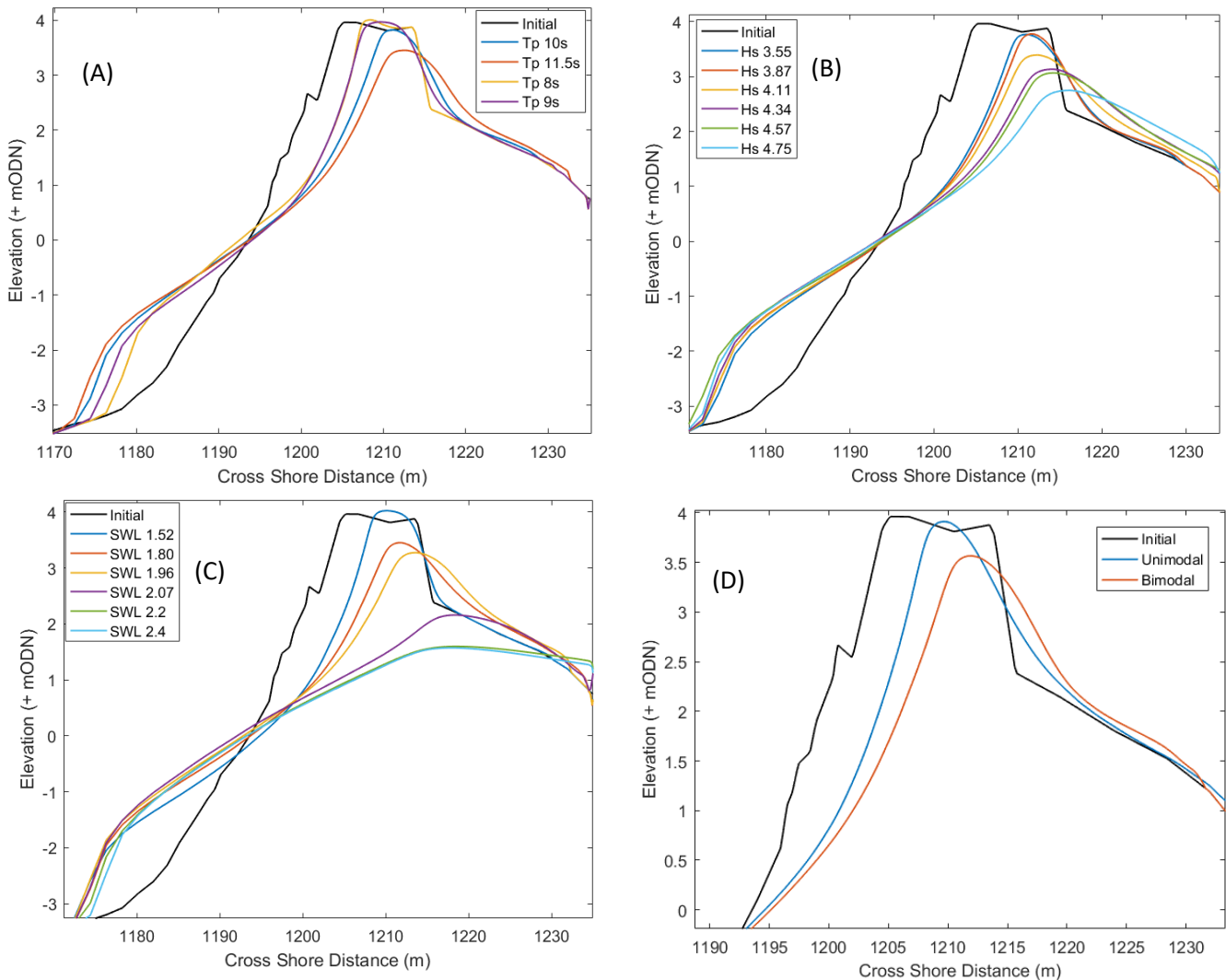
Figure 6.1- Cross shore profiles (ref Fig 5.3) of Cross shore 2 ,HS2- (A) Observed impact of peak wave period, Tp, with constant ESL of 1.52 and constant Hs of 3.64. (B) Observed impact of wave height, Hs, with constant peak wave period Tp of 10s and constant ESL of 1.52. (C) Observed impact of ESL,

constant wave height Hs of 3.64 and constant peak wave period, Tp, of 10s. (D) Observed impact of bimodal conditions compared with unimodal conditions, for Hs of 3.64, Tp = 10s and SWL of 1.05m comparing unimodal spectrum to 50% swell component.

6.2 Barrier Morphodynamic Responses

To investigate the morphodynamic response of the gravel barrier, 880 realisations of barrier responses under unimodal wave conditions and 36 responses under bimodal wave conditions were carried out, refer to table 5.1. Several modes of barrier response observed, which were categorised using the barrier response conceptual model of McCall et al. (2015) as shown in Figure 6.2:

(a)   *Beach face erosion* – For wave heights just above the storm threshold height (2.74m) combined with small peak wave periods (Tp<9s), where storm surge did not significantly reduce barrier freeboard (Rc), wave run up was confined to the swash zone. This resulted in sediment transported predominately offshore hence eroding the beach face (Figure 6.2a). Similar observations were found in Sallenger (2000);

(b)   *Crest accumulation* - In cross sections with small freeboard and/or barrier area, crest build-up due to overtopping was observed under moderate storm conditions. A similar process was observed in profiles with larger freeboard under higher energy storm conditions. In both cases sediment was typically transported up the beach face due to an increased run-up and deposited on the barrier crest (Figure 8b). This process reduced the width of the barrier. Gravel sediment transport on beach face is well described by (Austin & Buscombe, 2008). Bradbury and Powel (1993) states that crest accumulation can occur when a barrier is rolled over and, a new crest may form at a higher elevation and behind the original location of crest if there is sufficient sediment in the system. However, our results did not show evidence of this process;

(c)   *Crest lowering* - When energetic storm wave conditions (particularly with large wave periods) coincided with large surges, wave run-up exceeded the barrier freeboard and sediment was overwashed and deposited at the back of the barrier. As a result, the barrier crest lowered and the width increased (Figure 6.2c). It was also observed that waves with low steepness increased overtopping. There were several cases where the crest was lowered through avalanching of the barrier beach face;

(d) *Barrier Overwash* - Once a barrier had started experiencing overwashing, the general trend was that an increase in surge, H_s and T_p resulted in more overwash, leading to more sediment being deposited further behind the barrier (Figure 6.2d). The larger values of T_p resulted in sediment deposited further away from the back of the barrier. If ESL is significantly large, overwashing occurred even during low wave energy conditions. When the most energetic storms combined with largest storm surges overwash sediment was deposited far behind the barrier thus losing sediment from the active barrier morphodynamic system. As a result, the barrier may be more vulnerable to future wave attack, with long term effect being landward translation of the barrier, unless coastal management interventions take place.
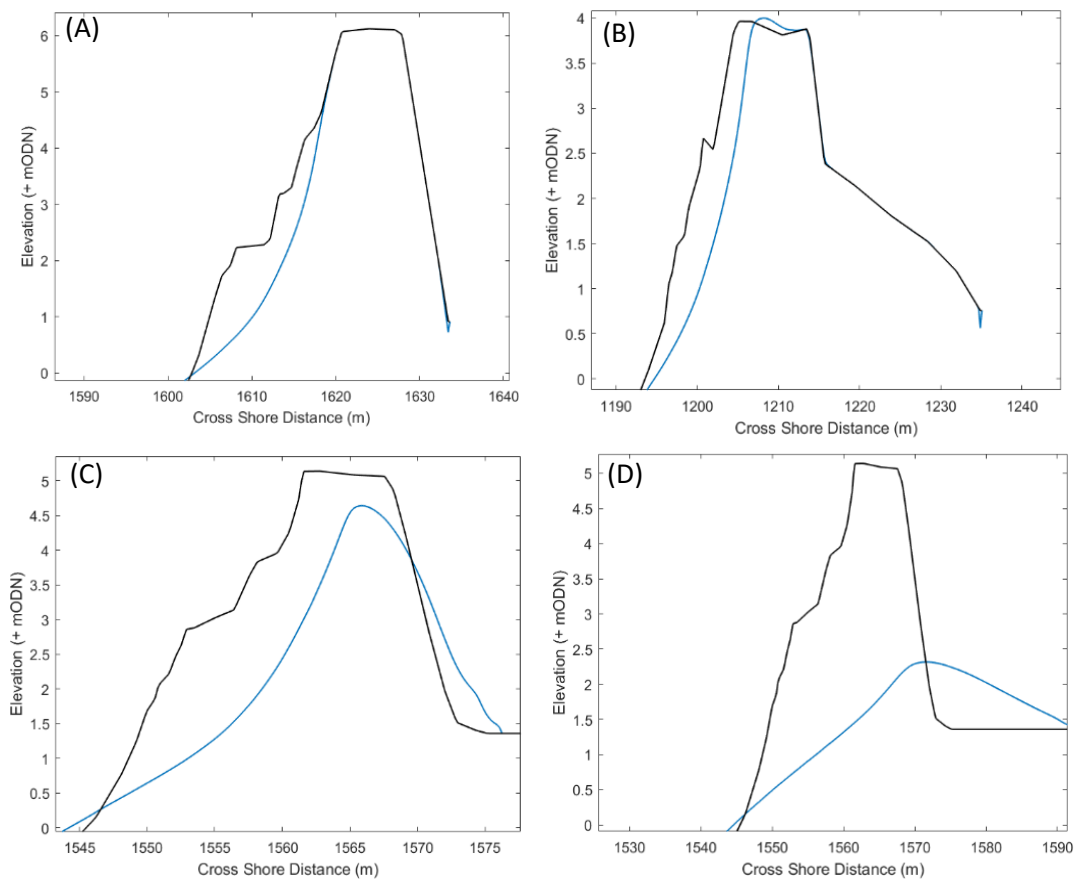

Figure 6.2 – Observed morphodynamic responses of the barrier beach to storm events, from the simulated results. Black line- Pre-storm, Blue line – Post-storm. (A) Beach face erosion; (B) Crest accumulation; (C) Crest lowering; and (D) Barrier overwash. Cross shore distance is 0m at the offshore boundary in XBeach model domain.

Other observations of barrier morphodynamic response were as follows: Barrier overtopping and/or overwashing was unlikely when both B_a and R_c are large; when B_a is large but R_c is small, the barrier was more prone to overwashing. Cases with a small B_a coupled with small R_c, experienced similar overwashing to that with large B_a and small R_c. This highlights the importance of R_c as an essential defence against extreme run-up that can occur during high surges. B_a appears to be of significance in controlling how soon the barrier becomes susceptible to overwashing events whereas smaller values of B_a can result in overwashing occurring earlier.

Bimodal impacts on HCS were observed to be the increase in magnitude of barrier response and also, more importantly, altering the mode of barrier response as seen in Figure 6.2(D). Where a barrier cross section was not previously susceptible to overwashing, bimodal conditions with high swell percentages were capable of producing severe overwashing events on the same barrier cross sections.

To capture the barrier response of HCS an approach similar to Bradbury (2000) and Bradbury et al. (2005) was used by coupling key hydrodynamic and geometric variables. Through an extensive literature and underlying physical process theories, the following variables were identified as key in gravel barrier beach processes. The storm extreme sea level (ESL), *Hs*, *Tp* were taken as the key hydrodynamic parameters while B_a, R_c and Z_c were taken as key barrier geometric parameters. Bradbury (2000) found that overtopping would be likely to occur when *Rc/Hs<1.1,* making inclusion of the term important for estimation of overwashing volume.

The output results Volume change, Overwash Volume and Crest change were calculated by comparison of pre-storm barrier topography and post-storm barrier topography. Figure 6.3 gives a visualisation of parameters and the method used. Volume change captures the face erosion (offshore sediment transport), as well as overwashing. When there is small overwash and sediment is transported on to the saltmarshes but, staying in the active barrier system, then it is included in post storm barrier volume. In cases where sediment was overwashed and deposited beyond the active part of the barrier, as seen for example in 1989 storms where Overwash Fans extended 80m's (Nicholls 1985). This is visualised as 'Overwash #2' in Figure 6.3. This sediment is considered to be lost from the active barrier. The reasoning behind this is once sediment is deposited beyond the 'active barrier' it is no longer contributing as part of the active defence- this sediment is effectively lost from the system as there are no natural ways of restoration.

Using Figure 6.3, Volume change is calculated as:

$$\Delta Vol = Initial\ Vol_{active} - Post\ storm\ Vol_{active} \quad (6.1)$$

Overwash Volume is calculated as the sediment deposited behind the back of the barrier, which is seen by the shaded areas of Overwash #1 and Overwash #2 in Figure 6.3.

Crest change, ΔZc , is calculated as:

$$\Delta Zc = Zc_{initial} - Zc_{post-storm} \text{ (6.2)}$$

In order to better categorise the observed barrier responses based on the controlling key parameters, a series of non-dimensional parameters were derived using Buckingham-Pi theorem and parametric testing. In total 6 variables were considered; significant wave height, *Hs;* peak wavelength*, Lp;* emergent barrier cross section above ESL*, Ba*; crest freeboard, which is the height of the crest above the ESL*, R*; initial crest height above 0 mOD*N, Zc* and initial barrier volume above 0 mODN *Vol.* Numerous non-dimensionalised relationships were established and parametrically tested, one of which includes the Barrier inertia parameter (B_i) of Bradbury et al. (2005) given in Equation (6.3):

$$\frac{RcBa}{Hs^3} = Bi \quad \text{(6.3)}$$

B_i has already been used to at numerous previous occasions to predict if barrier overwash/breach is likely to occur on gravel beaches. It includes the importance of extreme sea level on barrier response, making it appropriate for use also in this study. *Full geometric layout is given in on page 44 in Figure 5.3.*
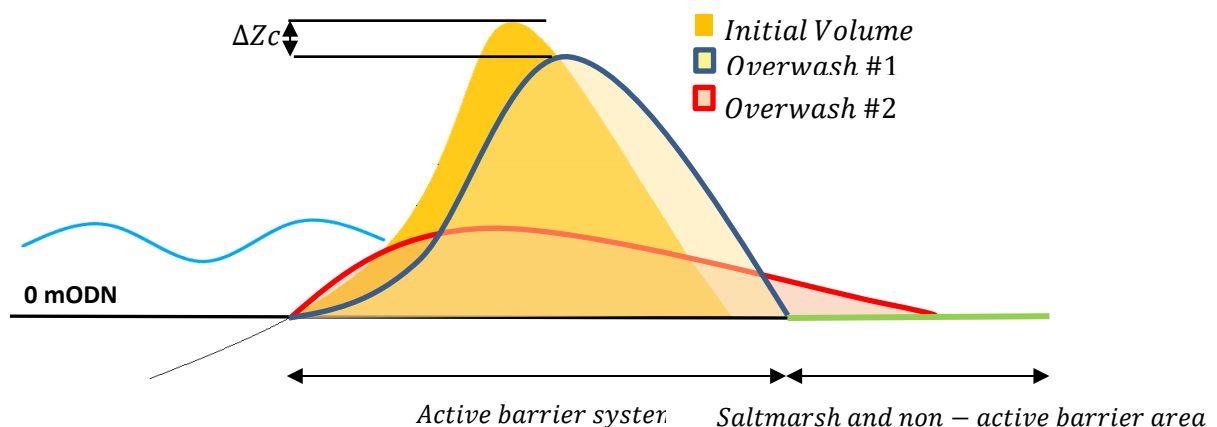
Figure 6.3 – Schematisation of output parameter calculations. Showing theoretical post storm profiles.

6.3 Volume Change

Figure 6.4 shows non-dimensional barrier volume change per metre length against Bi. In Figure 6.4(A), barrier volume change is non-dimensionalised by initial volume of the barrier per metre length (*Vol)* which offers a practical, easily understandable range in the y-axis giving volume change as a percentage of initial volume. However, as a result of the data scatter in this figure, it is difficult to identify a correlation between the *x* and *y* parameters. In Figure 6.4(B), the barrier volume change is non-dimensionalised using Z_c^2 which shows far greater correlation, with less data scatter. In an attempt improve the correlations, wave steepness $Hs/$Lp, was also included as seen in Figure 6.4(D). Wave steepness has been shown to significantly increase wave run-up on gravel beaches (Bradbury, 2000; Bradbury et al., 2005) as well displaying a clear impact on the beach profile as discussed in the initial observations. It can be seen that there is a large improvement with less scattering of the data observed.

The inclusion of wave steepness in Figure 6.4 (D) resolves the previous issues of data separating into distinct groups*.* Inclusion of wave steepness in Figure 6.4 (C) has reduced clustering of data into 2 distinct groups. whilst the fit in Figure 6.4(D) is not perfect, it is the strongest of all the fits trailed. The results from the least squared regression models for the best option given in Figure 6.4(D) can be seen in Table 6.1.
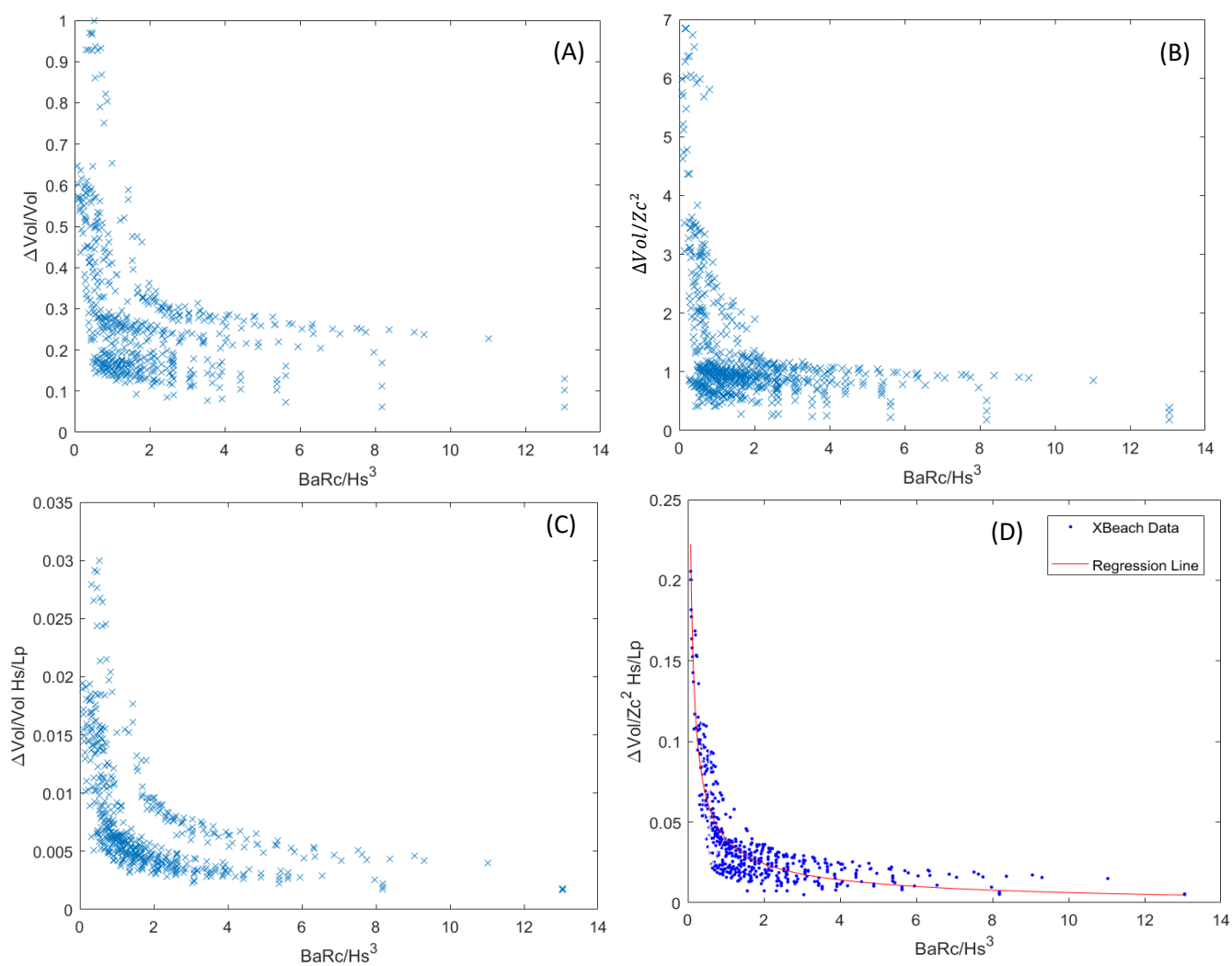
Figure 6.4 – Non-dimensionalised parameter scatter plots for change in barrier volume ΔVol for a range of different non-dimensionalisation attempts. 'Vol' is initial pre-storm barrier volume (A) Non-dimensionalised $\Delta Vol/Vol$ vs Non-dimensional Barrier inertia parameter, $BaRc/Hs^3$. (B) Non-dimensionalised $\Delta Vol/Zc^2$ vs Non-dimensional Barrier inertia. (C) $\frac{\Delta Vol}{Vol}\frac{Hs}{Lp}$ vs $BaRc/Hs^3$, (D) $\frac{\Delta Vol}{RZ}\frac{Hs}{Lp}$ vs $\frac{BaRc}{Hs^3}$,Regression model for Non-dimensional barrier volume change above 0m ODN per meter length of the barrier a during storm, red line shows regression curve.

Table 6.1- Goodness of fit statistics for initial least squared regression for Figure 6.4A SSE is sum of squared errors, r^2 is the proportion of variance for a dependent variable explained by the independent variable , RMSE is route mean squared error of residuals.

SSE	0.0824
r^2	0.7829
RMSE	0.0117

The regression line in Figure 6.4(D) can be seen to have produced a strong score with the Goodness of fit statistics (GOF). The r^2=0.7829 and RMSE 0.0117 are high showing considerable correlation of data points. However, goodness of fit statistics alone can be misleading and are insufficient to draw a full conclusion.

When the residuals for regression seen in Figure 6.4(D) are analysed further it highlights the underlying issues with the model as seen in Figure 6.5. Figure 6.5(A) shows a roughly normal distribution, however there are extreme values skewed towards the right with maximum residual of 0.08 compared to -0.04. This is confirmed in Figure 6.5(B), where heavy tailing is observed due to the occurrence of extreme residuals. Figure 6.5(C) shows the large scattering in the y-axis and heteroscedasticity. A common method to convert non-linear data and solve heteroscedasticity is the transformation of data. They include Log transformation, square root, cube root transformation and inverse of x-values and y-values. In this case, it is desirable to use the method that manipulates the data least, to allow the predictive model to be user-friendly without any back transformation required. Therefore, the square route method was selected and trailed below. After applying a square root transformation to the data the tailing in residuals is solved as well as the residuals becoming approximately normally distributed resulting in higher confidence in predicted values. The resultant regression can be seen in Figure 6.6 and the residual plots can be seen in Figure 6.7.
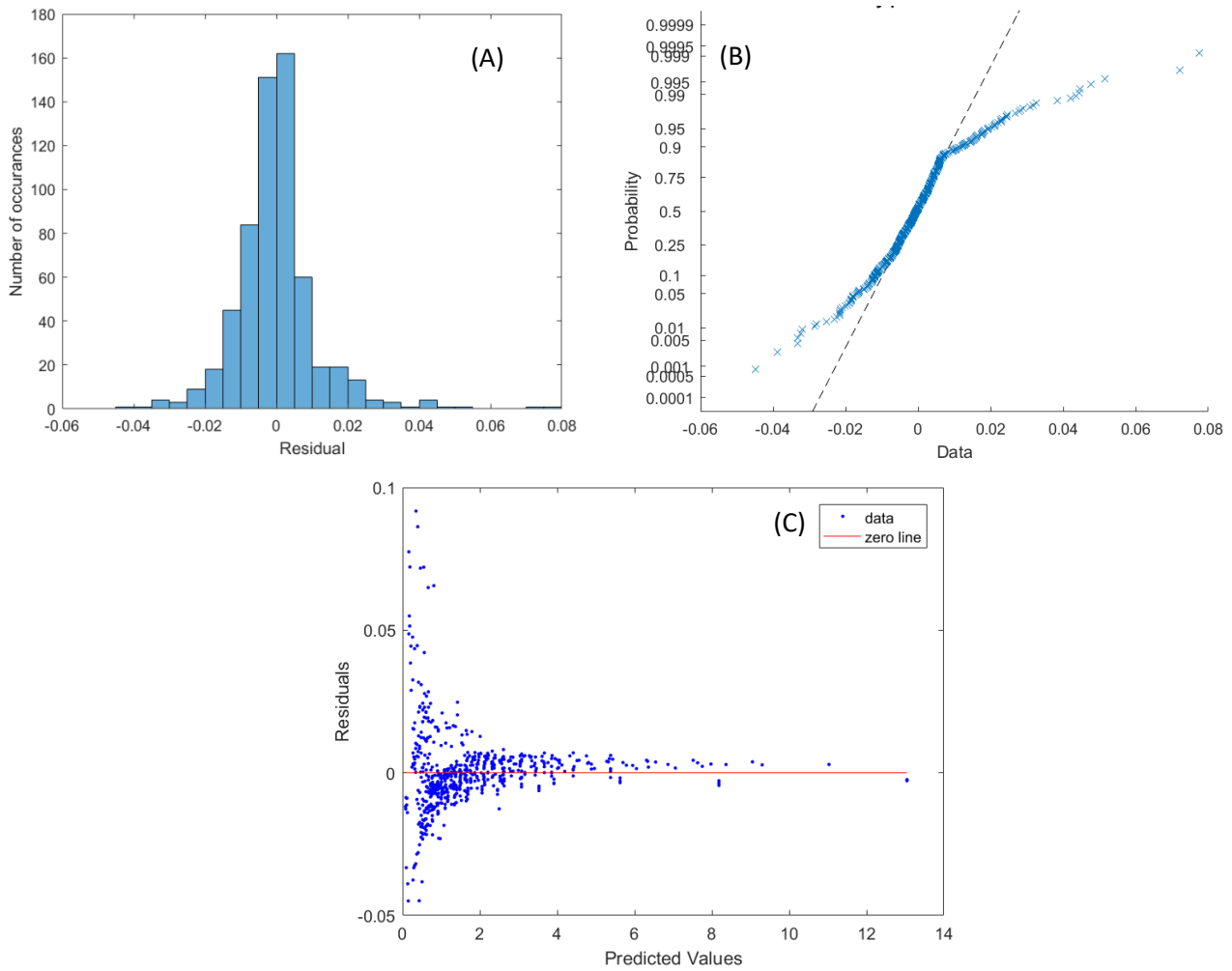
Figure 6.5- *(A) Histogram plot of residuals, (B) probability percentage of normal distribution plot, (C) Residual plot vs Predicted values.*

In Figure 6.6, the simulated non-dimensional barrier volume change above 0m ODN per metre length of the barrier is shown against the square root of the barrier inertia parameter (B_i). The results show a clear trend where smaller B_i give rise to larger barrier volume change. The exponential trendline derived using regression analysis and the 95% confidence intervals are also shown. The goodness of fit statistics in Table 6.3, highlight the strong correlation of the data to the best fit line. The regression line, which has a r^2 = 0.82 and RMSE=0.0126, is given by the equation:

$$\frac{\Delta Vol}{Zc^2}\frac{Hs}{Lp} = 0.02655\left(\frac{RcBa}{Hs^3}\right)^{-1.06} + 0.01 \qquad (6.5)$$

The valid range of the regression equation should not exceed the physically modelled bounds:

$$0.27 < \frac{RcBa}{Hs^3} < 13 \qquad (6.6)$$

and
$$0.0133 < \frac{Hs}{Lp} < 0.047 \qquad (6.7)$$

It may be useful if the regression line given in Equation (6.5) can be used as a predictor to estimate change in barrier volume during single storm events, which can serve as a simple parametric model. To check the validity of the model for conditions outside those used for numerical simulations, barrier volume change measured at several cross sections of HCS and SSBB located in the south-west of the UK during a range of storms were used (Table 6.2). The historic pre- and post-storm barrier cross sections and, storm wave and water level data are provided by the Channel Coastal Observatory of the UK, Bradbury (2000), Bradbury et al. (2005), McCall et al. (2013) and Chadwick et al (2005). Hurst 1a and Hurst 1b represent two separate cross sections of HCS which were derived from previous literature, Bradbury (2000), using historical storm data from a 1989 storm. During the 1989 storm event large overwashing and breaching of HCS occurred. Hurst 2 represents a single cross section from hindcast storm data derived from CCO data. Hurst 3a and 3b represent 2 cross sections from the same storm derived from CCO data. Finally, Slapton1-3 are three different cross sections from the same storm, also derived from CCO data.

Table 6.2 – Volume change measured at cross sections along HCS and Slapton beach during storm events, used to validate Equation (6.5).

Validation case	H_s (m)	T_p (s)	Extreme Sea level above ODN (m)
Hurst 1a	2.9	10.96	0.87
Hurst 1b	2.9	10.96	0.87
Hurst 2	3	12.6	1
Hurst 3a	3.95	12.3	1.27
Hurst 3b	3.95	12.3	1.27
Slapton 1	4.87	8.3	1.905
Slapton 2	4.87	8.3	1.905
Slapton 3	4.87	8.3	1.905

The results reveal that two validation cases are outside the validity of the parametric model $\left[\frac{RcBa}{Hs^3} > 13\right]$. However, those cases resulted in very small barrier volume change and therefore, not significant. Four validation cases fell within the 95% confidence limits showing good degree of accuracy of the model while 2 cases were outside 95% confidence limit (Figure 6.6). Although further validation is necessary before the parametric model can be widely used as a predictor, these results give reasonable confidence to use it to estimate the changes in gravel barrier volume during storm events.
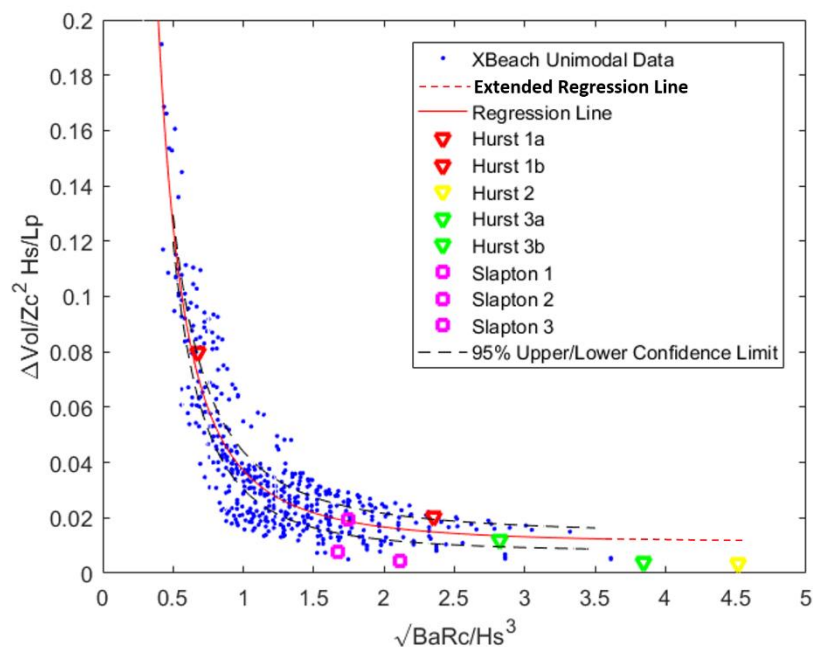
Figure 6.6 - Non-dimensional barrier volume change above 0m ODN per meter length of the barrier a during storm against the square root of the barrier inertia parameter (B_i). The exponential regression trendline is given by the red line. 95% confidence limits are shown by the broken black line. The regression line validation data at HCS and Slapton Barrier beach are shown in green, yellow and red triangles and purple squares. The red dashed line shows the extended range of the model to cover the validation cases of Hurst 2 and Hurst 3a.
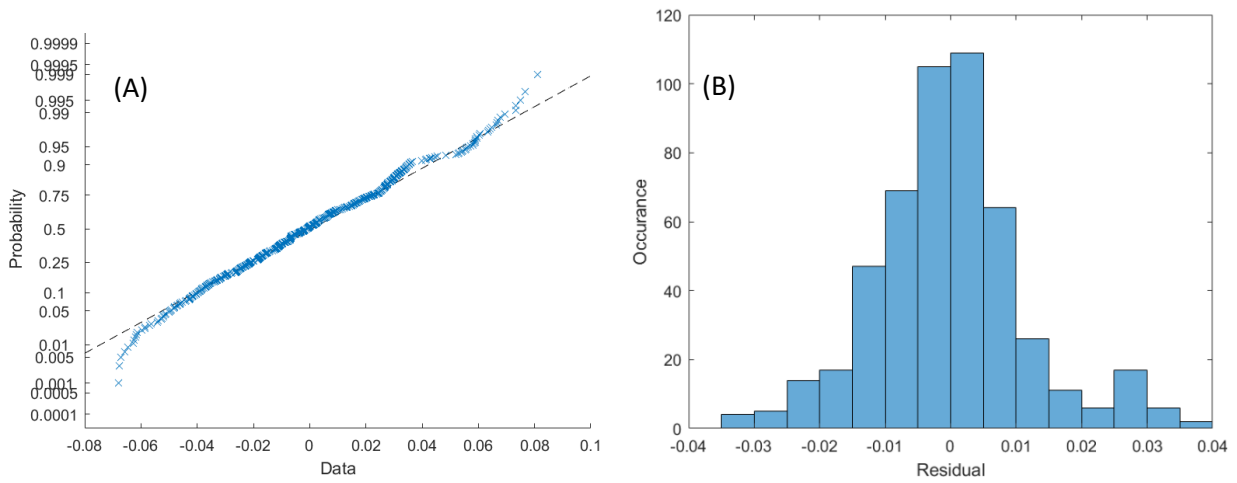
Figure 6.7- Residual plot analysis for transformed volume change regression seen in figure 6.6. (A) Probability percentage plot for normal distribution, where X-axis is residual data. (B) Histogram plot of residual distribution.

Table 6.3- Goodness of Fit statistics for regression model displayed in Figure 6.6.

SSE	*0.0802*
r^2	0.82
RMSE	0.0126

6.4 Overwash Volume

First attempts to build a parametric model for Overwash Volume (*OV),* included the use the same methodology and parameters as in barrier volume change model in Eq. (6.6). Figure 6.8(A) and Figure 6.8 (B) both show very similar non-linear trends with strong correlation, however as Figure 6.8(B) shows the inclusion of *Hs/Lp* increases the r^2 from 0.52 to 0.65. There is one outlier in green which has been identified and removed from both models. Both models trendlines clearly overpredict overwash volume for *Bi* <4, where the majority of the data falls. There is also a large amount on zero value which have a significant impact on the distribution of the residuals, which must be Normally distributed for predictive purposes. This is shown in Figure 6.9.

Figure 6.9 shows the residual analysis for Figure 6.8 (B), '*OV/Zc^2 Hs/Lp vs BaRc/Hs$^{3'}$.* The non-normal distribution of the data is clear in Figure 6.9 (A) &(B), the heavy tailing of the residuals shows the extreme values are not correctly captured. Figure 6.9 (C) shows a clear exponential trend in the negative y-axis which is due to the constant variance between the zero values and the regression curve. There is also large heteroscedasticity of the data. In order to normalise the residual data, a square root transformation was applied for volume change, however the zero values restrict any transformations being consistent. Therefore, by removing zero values, a square root transformation could be applied. The result of which can be seen in Figure 6.10. Figure 6.10(A) has a slightly lowered r^2 with zero values removed, however there were 200+ zero values and the larger *n* data points is, the higher an r^2 is also. The biggest improvement is seen in the distribution of the residual values, however normal distribution is still not achieved.

Further development of the model can be achieved by taking square root transformation of the data. This is shown in Figure 6.11, The r^2 value increased to 0.7 with the transformation, as well as a lower, more favourable RMSE value. Despite the Goodness of fit improvements, the distribution of residuals is still unsatisfactory for prediction purposes due to the skewness in the upper probabilities of residuals shown in Figure 6.11(B).

No further improvements were possible when using the previously discussed parameters, therefore a new set of non-dimensionalised parameters, shown in Figures 6.12 and 6.13 were investigated to explore if a better correlation between Bi and barrier overwash volume can be found.
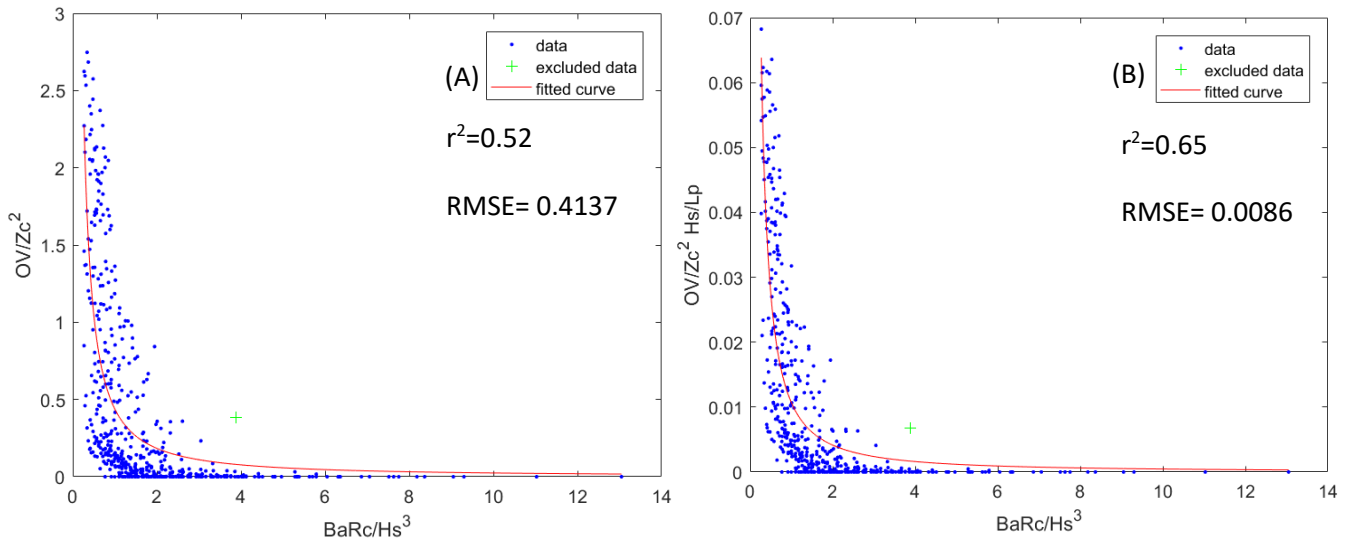
Figure 6.8 - (A) and (B) show non-dimensional regression models for sediment overwash m² volume per metre unit width.
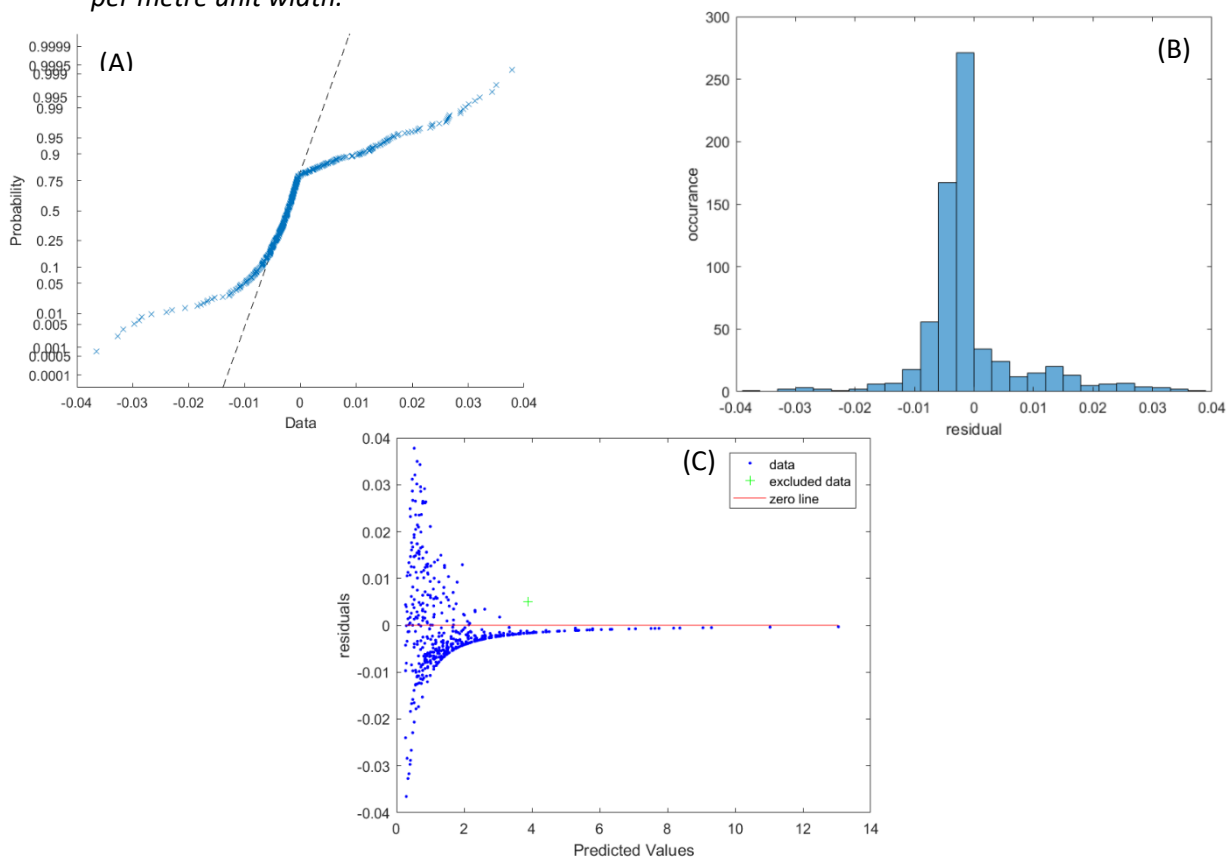
Figure 6.9- Residual Plot analysis for regression results in Figure 6.8 (B). (A) Probability percentage plot (B) Histogram of residual distribution (C) Residual vs Precited values
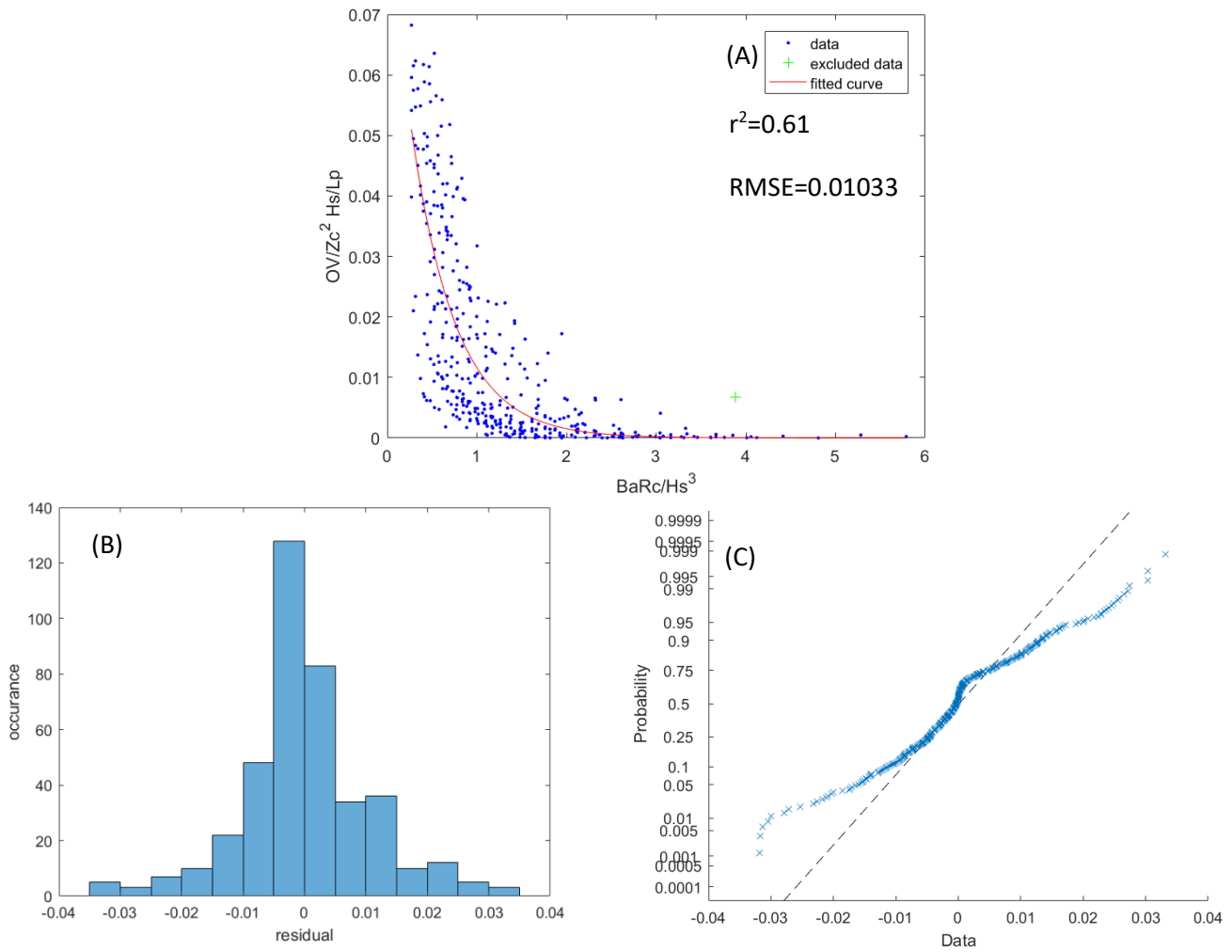
Figure 6.10 - Regression results and residual plots when zero overwash values removed. (A) Exponential regression model for non- zero data, (B) Probability histogram, (C) Probability percentage residual plot
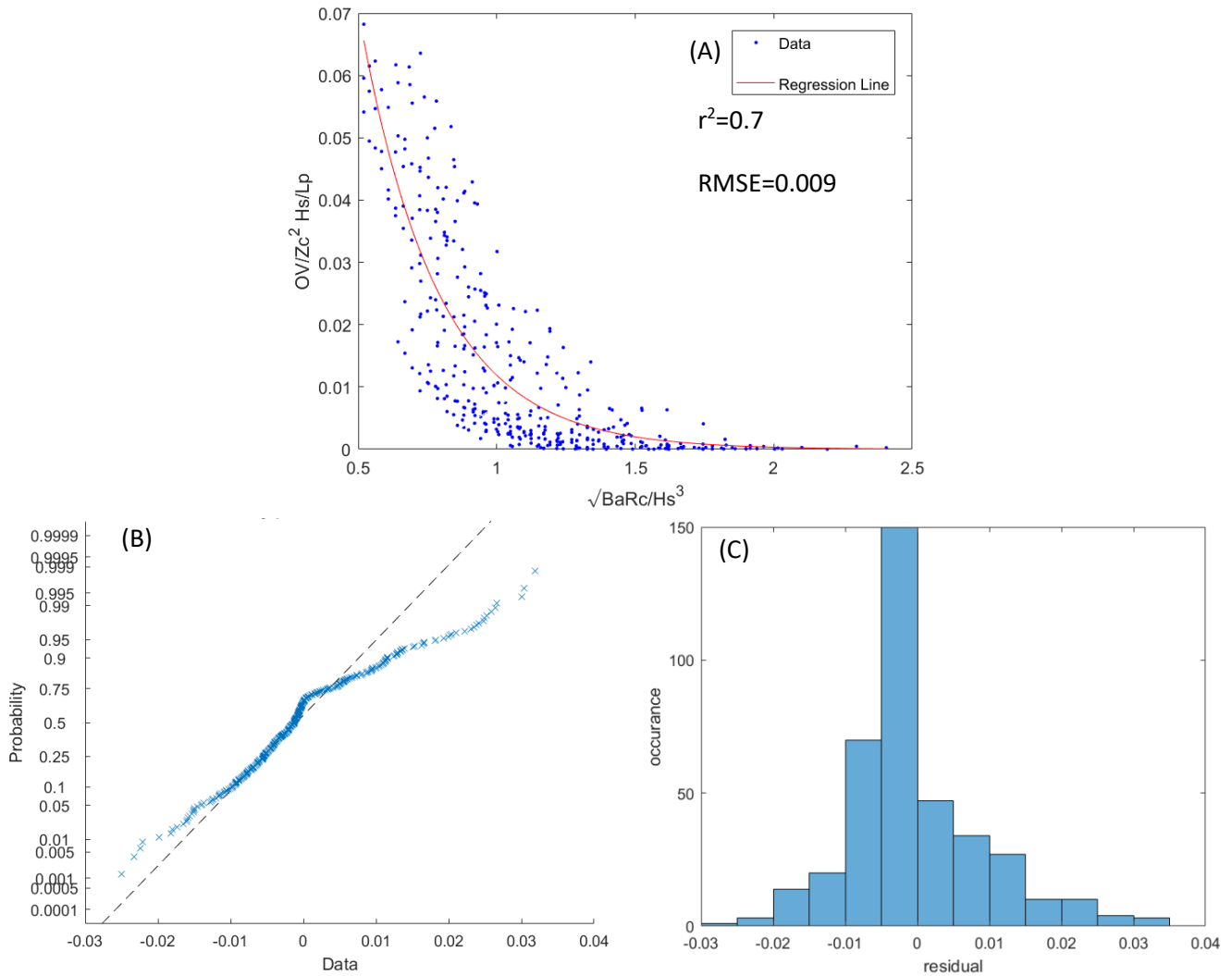
Figure 6.11- Regression results and residual plots when zero overwash values removed, and x-axis data transformed via square route transformation. (A) Exponential regression model for non-zero data, outliers have been removed from raw (B) Probability histogram, (C) Probability percentage residual plot

In Figure 6.12, all y-axis values in the right column have had a square root transformation applied. This increased the range of distribution of data about the x-axis, reducing the gradient of the curve as it can be seen that the figures in the left side column have near vertical trend. A very strong correlation was found between *Hs*Lp*, although this parameter is not commonly used in practice due to the 'non-physical' aspects of the parameter. It can be described 'non-physical' as the vertical *Hs* is multiplied by horizontal *Lp*, however in the interest of building a predictive framework *HsLp* was used as a key parameter henceforth.

In Figure 6.12 (A) *Ba* is nondimensionalised by *HsLp,* and *OV* is non-dimensionalised by initial crest height, *Zc.* The Figure shows there is strong correlation and non-linear negative trend, it is clear that for larger values of *Ba/HsLp* there is no overwashing occurring. However, the zero values, as shown previously cause skewing to residuals distribution, therefore they were removed which can be seen in Figure 6.12 (B). Figure 6.12 (B) shows the exponential regression line $y = 2.39e^{-53.39x}$, with an r^2 value of 0.797.

The next set of non-dimensionalised parameter that were tried are seen in Figure 6.12 (C)&(D), where relative freeboard *Rc* was included due to the known importance in controlling overtopping processes (Bradbury 2000, Sallenger 2000). Figure 6.12 (D) shows the exponential regression line $y = 3.92e^{-39.07x}$, whilst the r^2 value improved to 0.8533 and RMSE decreased to 0.1696, highlighting the high correlation of the data and the low variation about the mean line. In comparison to Figure 6.12 (B), there is larger scattering of the results in *x* > 0.4. Overall there is limited observed change other than improvement in r^2 values. The last set of non-dimensional parameter combination is seen in Figure 6.12 (E) and (F). The Figure shows the square root of the overwash volume, non-dimensionalised by barrier freeboard - $\sqrt{OV/Rc^2}$ against *BaZc/Hs^{2}Lp,* hereafter referenced as *Bi2*. These results yielded the best correlation observed with an r^2=0.87.

Figure 6.12(F) was further analysed, seen in Figure 6.13. The residual plots highlight the improvement the new non-dimensional parameters have over previous attempt. Figure 6.13 (A) shows that the residuals are approximately normally distributed. Figure 6.13 (B) shows the distribution of probability plot is not exactly 45° however it is approximately normal. Figure 6.13 (C) shows the residuals are equally distributed about the regression line with random scattering of the residuals around the regression line and no trend visible. Although there appears to be some heteroscedasticity, this is due to less data available for larger *Bi2* values.
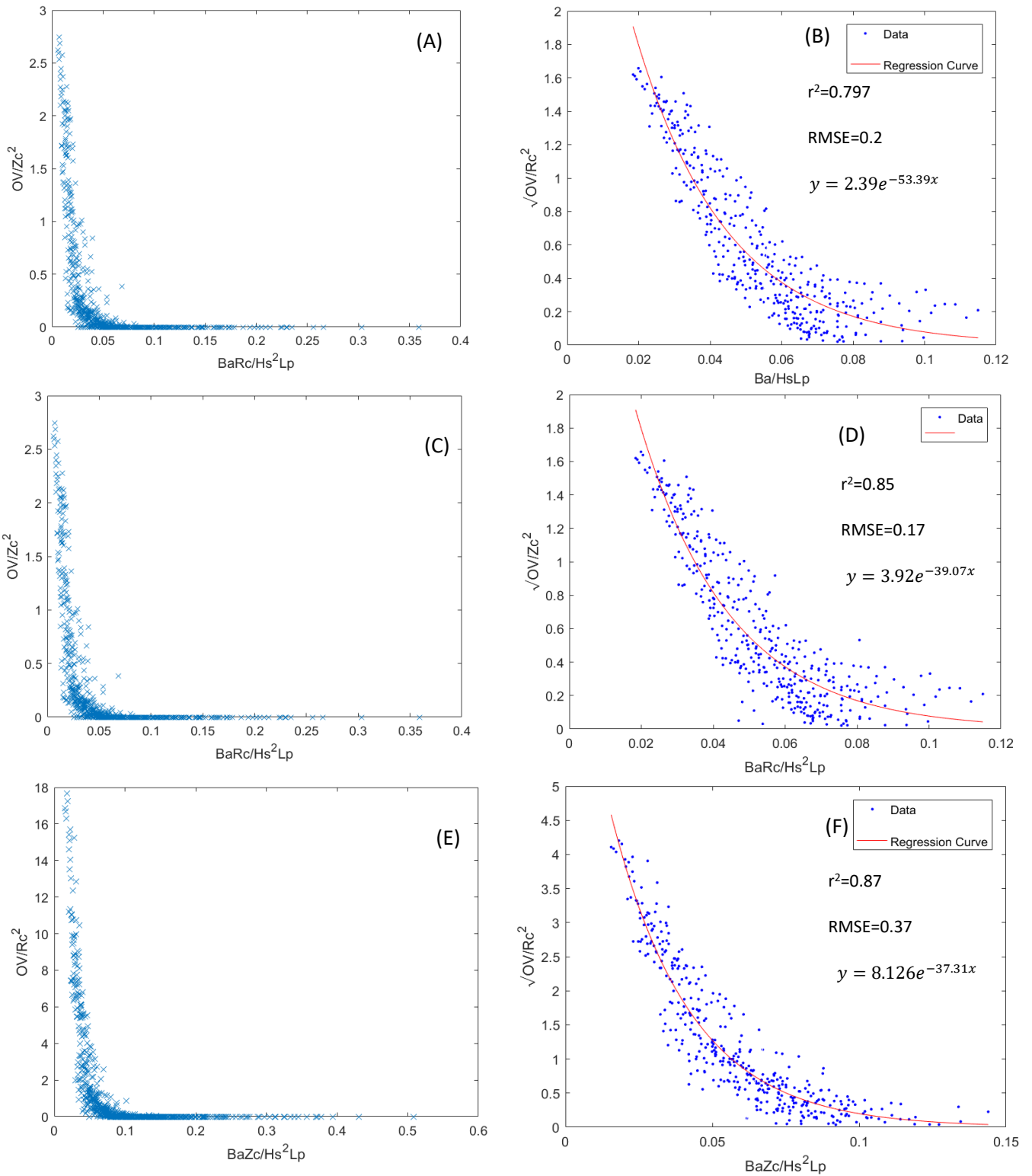
Figure 6.12- Left Column shows series of non-dimensionalised scatter plots exploring different combinations of non-dimensional parameter combinations to find best fit. Right column shows regression models corresponding to Left column figures, with zero values removed.
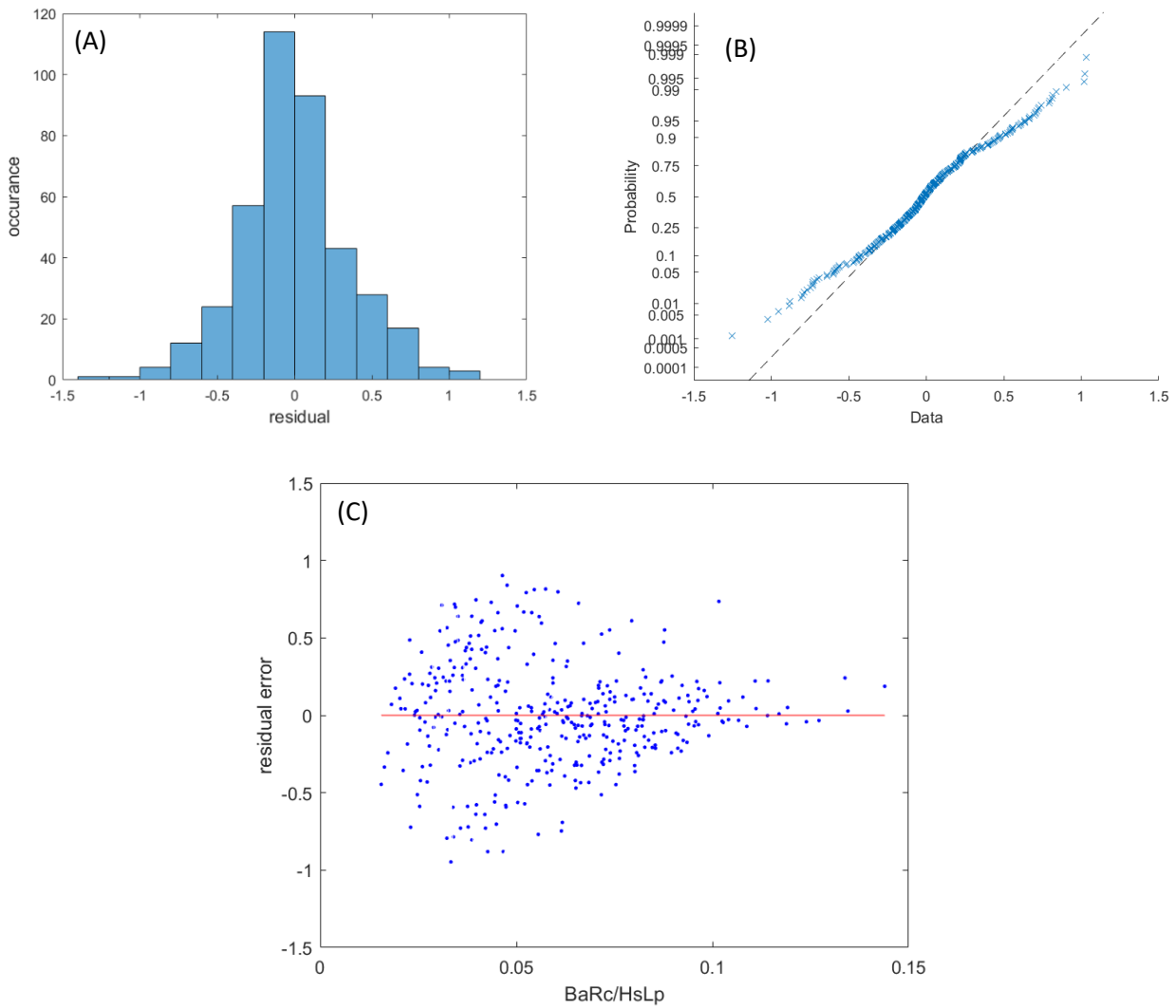
Figure 6.13 Residual Plot analysis for Figure 6.12(F). (A) Normal distribution plot of residuals (B)-Probability plot for normal distribution (C) residual plot vs predicted values.

In Figure 6.14, the final selected simulated non-dimensional Overwash volume per metre length of the barrier is given. The results show a clear trend where smaller *Bi2* give rise to larger overwash volume. The exponential trendline derived using regression analysis and the 95% confidence intervals are also shown. The regression line with r^2 = 0.87 is given by the equation:

$$\sqrt{OV/Rc^2} = 8.126e^{-37.31\frac{BaZc}{HsLp}} \tag{6.8}$$

the valid range of the regression equation is

$$0.02 < \frac{BaZc}{HsLp} < 0.15 \qquad\qquad (6.9)$$

The regression line given in Equation (6.8) could be used as a predictor, after some further development, which can serve as a simple parametric model to estimate barrier overwash volume during storms. To check the validity of the model for conditions outside those used for numerical simulations, barrier overwash volume change measured at several cross sections of HCS and the Slapton barrier beach located in the south-west of the UK during a range of storms were used (Table 6.2). The historic pre- and post-storm barrier cross sections and, storm wave and water level data are provided by the Channel Coastal Observatory of the UK, Bradbury (2000), Bradbury et al. (2005), McCall et al. (2013) and Chadwick et al. (2005).

The results revels that the model has some skill in predicting overwash volume, albeit is less successful than that of barrier volume change model. The general trends are accurately captured by the trendline which is promising. Due to limited data available no measured overwashed events could be calculated using topographic data, therefore historical overwash events were estimated using literature for Hurst spit storm in 1989 (Bradbury, 2000). The red Hurst cases experienced no overwashing which is subsequentially overpredicted by the model, this could be down to the impact of removing zero values from regression, therefore higher values of $Bi2$ may be slightly over predict overwashing. The estimated overwash amount is however considerably small in these ranges. The historical data plotted in purple squares are both within the range of modelled data, however outside the confidence intervals. Whilst Slapton cases are outside the validity range of the regression model, they are within the XBeach modelled data, and correspond to the zero values seen in Figure 6.12(E), it can be assumed the mode predicts the correctly that no overwash is occurring for these sights. Although further validation is necessary before the parametric model can be widely used as a predictor, these results give reasonable confidence to use it to estimate overwash volume during storms.

There are however limitations to the applicability of the Overwash volume model described above. Firstly the model is unable to identify if there is no overwashing as a result of zero overwashing cases being removed during the model development. Secondly the due to the non-dimensional parameters being transformed through square root transformation, the confidence limits would also require transforming. This has not been developed in this thesis. Since the non-transformed data is not normally distributed then predictive assumptions are limited currently.

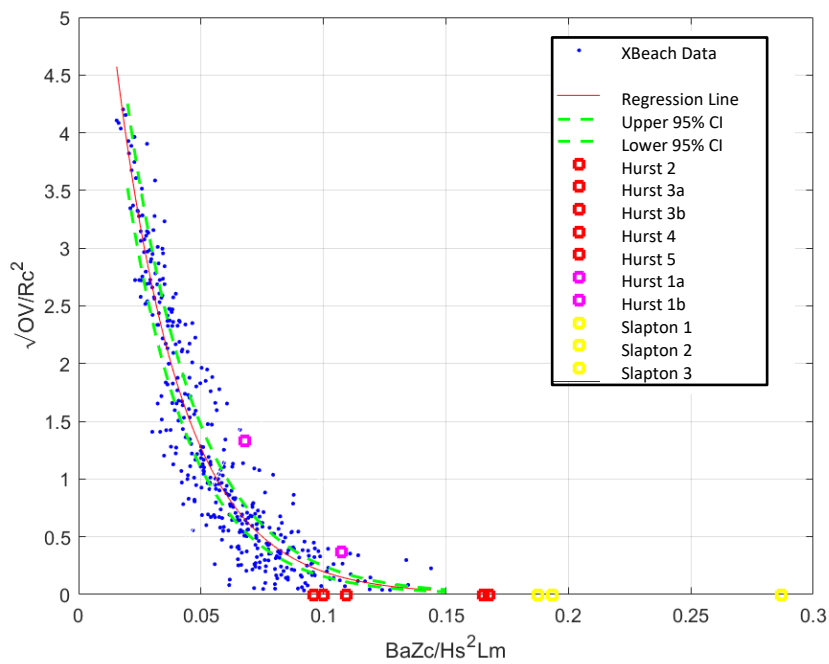*Figure 6.14- Non-dimensional Overwash Volume per meter length of the barrier a during storm against the BaZc/HsLp. The exponential regression trendline is given by the red line. 95% confidence limits are shown by the broken black line. The regression line validation data at HCS and Slapton Barrier beach are shown in green, yellow and red triangles and purple squares.*

6.5 Crest Change

Following the same approaches outlined in section 6.3 and 6.4, the crest change of the barrier was investigated. Crest change was non-dimensionalised by initial crest height, Zc, and the barrier inertia parameter (Bi) was found to give strongest correlation as shown in Figure 6.15. As aforementioned above Bi is used to great success in predicting overwashing of barriers, which can be directly linked to crest lowering processes. There is a strong correlation with the Bi parameter increasing and the change in crest height decreasing resulting eventual in no change. There is however large spreading in the y-axis where Bi<5, with values ranging from crest accumulation, crest lowering or no crest change as shown in Figure 6.15 (A).Figure 6.15 (B) shows the random nature of points about the 0 crest change line. This issue makes capturing the magnitude of response of crest change difficult through empirical model.

By fitting an exponential curve to Figure 6.16, the follow equation and Goodness of Fit statistics were derived:

$$y = -0.6297e^{-1.477x} \qquad (6.10)$$

Table 6.4 – Goodness of Fit statistics for regression equations (6.10)

SSE	14.99
r^2	0.41
RMSE	0.1578

Figure 6.16 shows whilst the trend line captures the observed exponential curve, it fails to pass through large portions of the data, which is reflected in the adjusted r^2=0.41, which is relatively low. RMSE value of 0.1578 is considerably large also. Further analysis of the regression model through residual analysis confirms the model is not good fit. Figure 6.17(A) and 6.17(B) show the normal distribution of the residuals, if there is a non-normal distribution of residuals it can be assumed predictions will be less reliable for this x-values. Figure 6.17(A) shows the heavy tailing of the data, this could be expected when modelling extreme events and a Weibull distribution could offer a better fit. However, when compared to the Exponential fit there was no significant improvement. Figure 6.17(C) shows the that the Y-axis is unbalanced as well as there being large Heteroscedasticity to the left-hand side of the data. There is also a clear trend captured above the 0 line, due to curve of the exponential falling to capture the linear trend of constant zero $\frac{\Delta Zc}{Zc}$ values. No attempts to use the data

transformation methods previously discussed for Volume Change and Overwash volume, due to the nature of the data collected, the zero values, positive values, and negative values all carried significant importance and could not be omitted.

In the future separating crest accumulation and crest lowering into 2 different groups, then analysing the trends in the data may provide more usable result and removing the random clustering of data as seen in Figure 6.15 (E). Another solution could be to only seek to provide a threshold, similar to (Bradbury et al., 2005), to indicate when a crest height will decrease from a resultant storm.
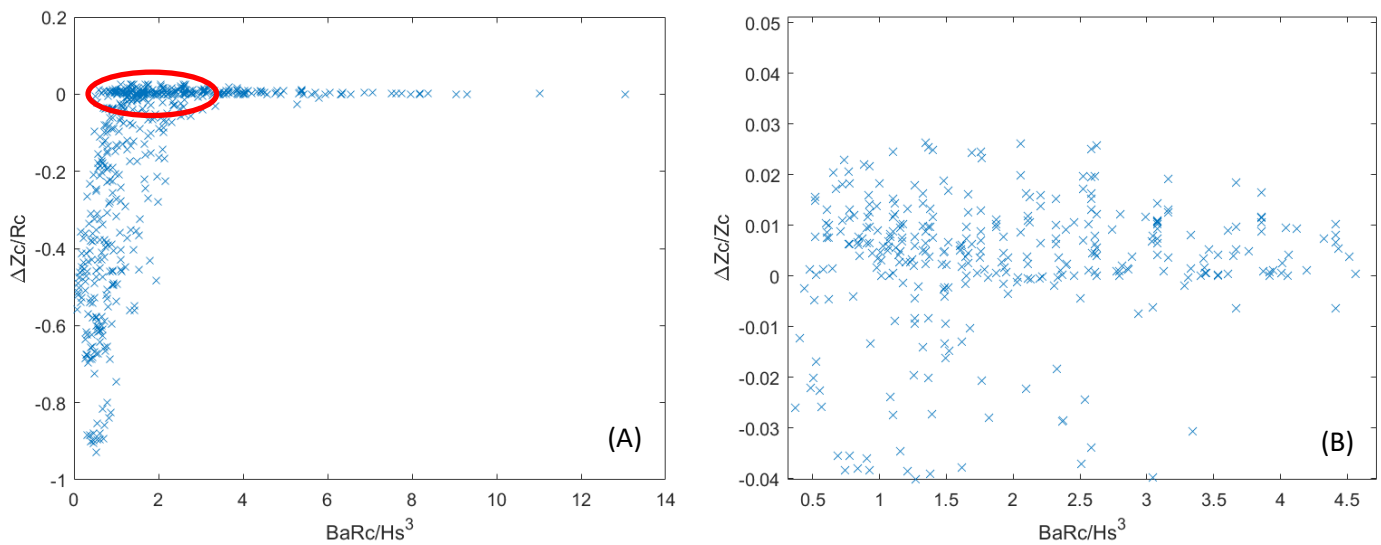
Figure 6.15- Scatter plots of coupled non-dimensional key hydrodynamic and geometric parameters tested for trends and correlation to Change in Crest height,ΔZc. (A) Non-dimensional change in crest height ($\Delta Zc/Zc$)., vs Barrier inertia parameter, Bi (BaRc/Hs^3). (B) Red circle in figure A is shown, which highlights clustering of data about y=0.
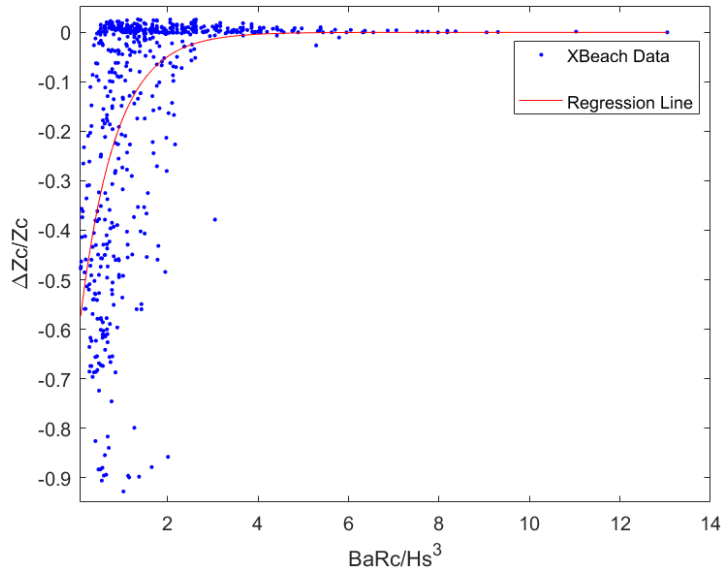
Figure 6.16- Exponential regression model for change in crest height v Bi. Eq (6.10)
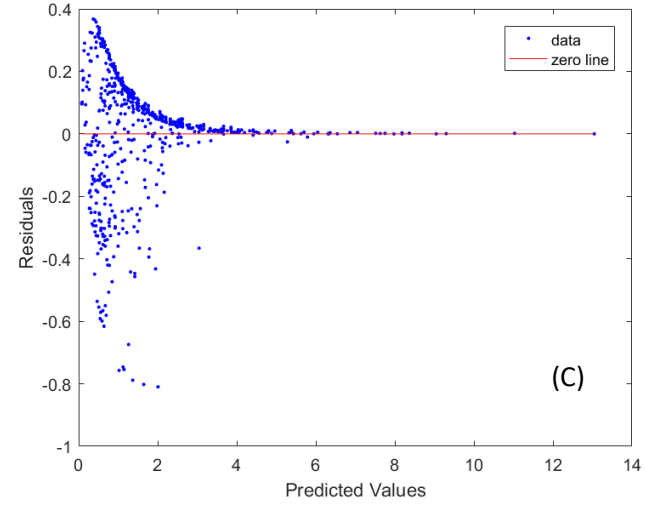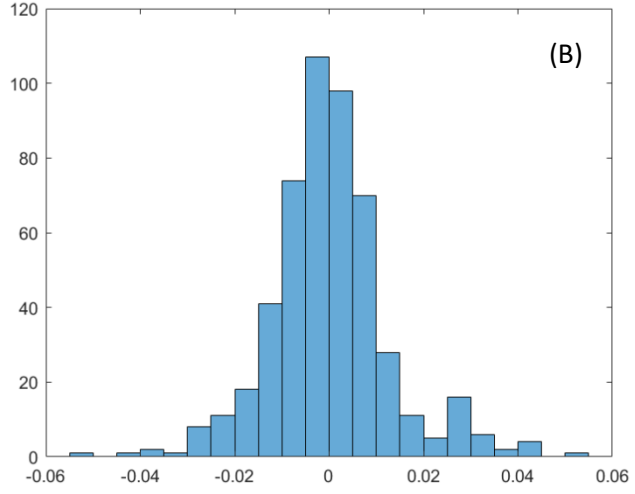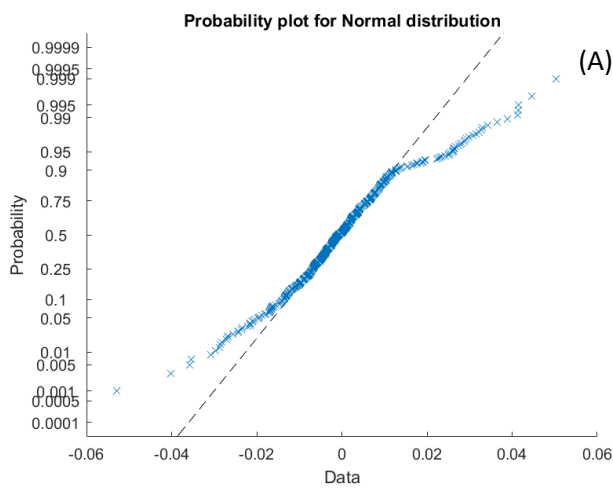
Figure 6.17 – Residual plot analysis of exponential regression fit in equation 6.10. (A) Probability plot for normal distribution. (B) Histogram for distribution of residuals. (C) Predicted values against residuals.

6.6 Bimodal Storm Conditions

Although the parametric model given in Equation (6.5), (6.8) and (6.10) are derived based on numerically simulated barrier volume change during unimodal storm conditions, it is well known that the south-west of the UK is subjected to frequent storms with bimodal characteristics as a result of swell-dominated waves reaching from the Atlantic.

To examine the impacts of bimodal storm conditions on gravel barriers, the model was used to simulate barrier volume change and overwash from bimodal storms. Bimodal spectra to derive offshore wave boundary conditions to the XBeach model, were determined using Polidoro & Dornbusch (2014) which using wave height, water levels and swell percentage given in Table 6.1. 36 realisations were modelled. The significant wave height Hs for bimodal waves was determined using.

$$Hs = \sqrt{H_{wind}^2 + H_{swell}^2} \qquad (6.11)$$

where H_{wind} is the significant wave height of the wind wave component and H_{swell} is the significant wave height of the swell wave component.

In Figure 6.18 the non-dimensional barrier volume change per meter length from bimodal waves are shown and compared with unimodal results. It can be seen that during bimodal storms with swell percentage greater than 40-50%, the non-dimensional barrier volume change for a given barrier inertia is larger than that of their unimodal counterparts, especially at low values of barrier inertia. There is a noticeable increase in volume change from storms with 50% and 75% swell conditions. On the other hand, if the swell percentage is less than 30% non-dimensional barrier volume change is less than that from the unimodal cases for a given barrier inertia.
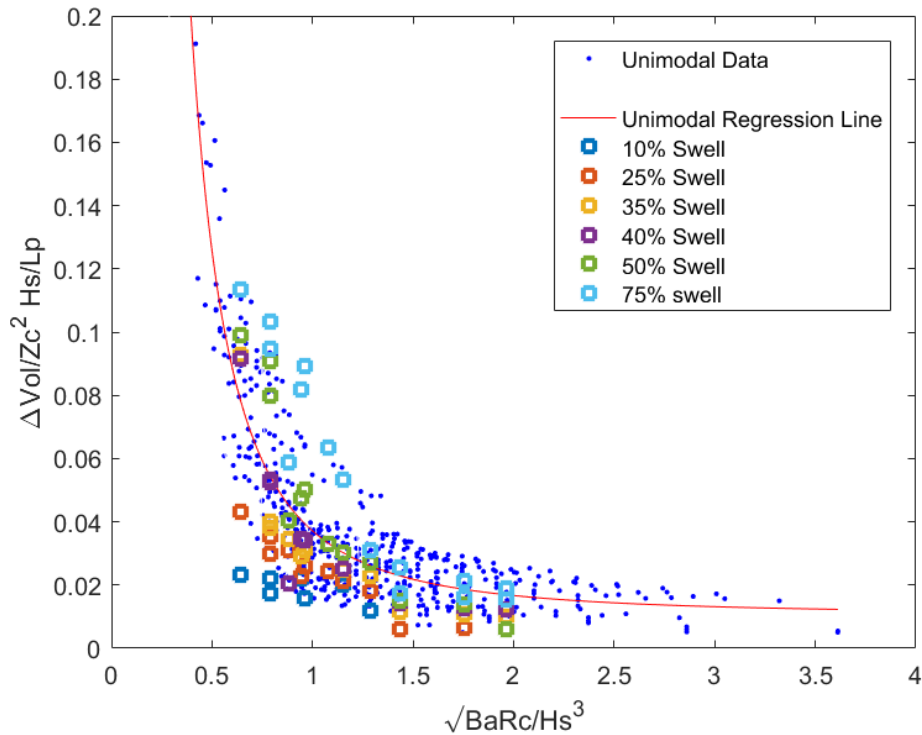
Figure 6.18 Comparison of unimodal and bimodal non-dimensional barrier volume change under different swell percentages. The red line is the parametric model given by Equation (6.5).

To examine the impact of wave bimodality on barrier response in more details, barrier volume change and overwash volume from storms under bimodal conditions at each individual cross section was investigated in isolation and compared with unimodal results. Figure 6.19 shows the results for cross section HS2, seen in Figure 5.1. The data was fitted with a curved line of best fit allowing for a comparison of each swell %. Figure 6.19 clearly shows that the increasing swell wave component leads to greater barrier volume change and larger overwashing volumes and that when swell percentage is greater than 40% the barrier volume change and overwash volume is greater than that from the unimodal waves, for the same freeboard.
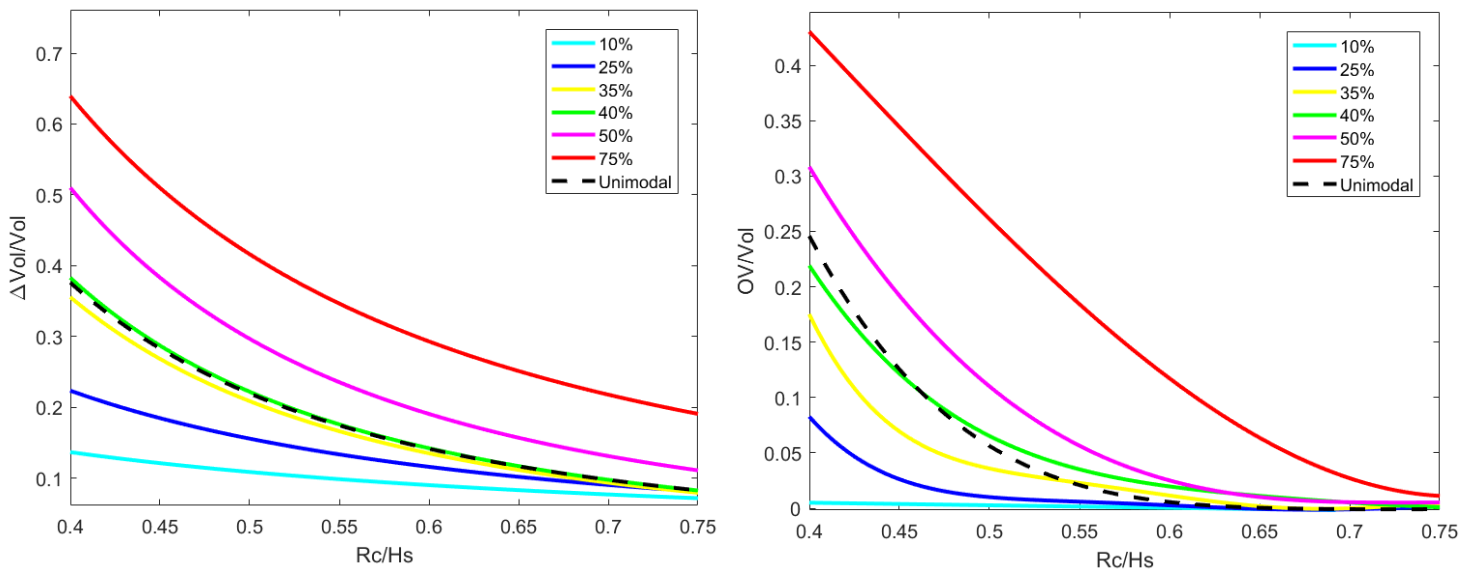
Figure 6.19- The effect of swell percentage of bimodal storm waves on barrier volume change (left) and overwash volume (right) for a single cross section , HS2. Δvol = barrier volume change per meter length and Vol = pre-storm barrier volume/meter length; OV = overwash volume.

Barrier beach overwashing is an important process which contributes to back barrier flooding as well as barrier response to storms. Therefore, the relationship between the overwashing volume and the barrier inertia parameter was also investigated. Figure 6.20 gives the simulated non-dimensional overwash volume from both unimodal and bimodal storm conditions. Although there is a significant data scatter, an overall trend of overwash volume reduction with increase barrier inertia can be seen. Also, similar to barrier volume change, overwash volumes from bimodal storms with higher swell percentages are significantly larger than that from unimodal storms under the same barrier inertia. During extreme cases where swell percentage is 75%, complete inundation of the barrier has taken place and a significant volume of sediment has been removed from the active barrier beach and transported further away from the back barrier. An event like this has been recorded at HCS where the barrier has breached following a storm in 2005 (Bradbury et al. 2007). On the other hand, storms with less than 25% swell component gave rise to very low overwash volumes.
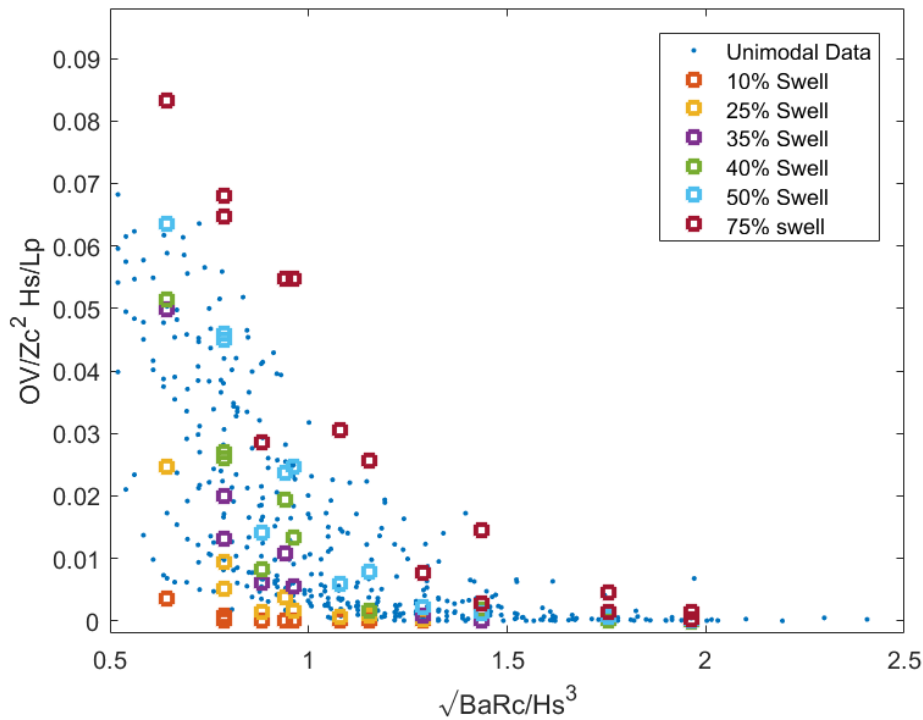
Figure 6.20- A comparison of simulated barrier overwash volumes from unimodal storms and bimodal storms with varying swell percentages.

A probable reason for 'positive' and 'negative' swell effects on the barrier response and overwashing may be explained by different behaviours of wind and swell waves. Short period wind waves dissipate further away from shore due to shoaling and steepening of the wave. This may limit the potential wave run up and wave energy reaching the barrier beach face. On the other hand, longer period swell waves, with their low wave steepness, can dominate the surf zone and propagate closer to the beach face without dissipation due to breaking (Masselink et al. 2014; Almeida 2017). If the swell percentage is small, wind waves dominate the surf, swash and runup while the contribution from swell waves may be small. For sea states with larger swell components, undissipated swell waves dominate large runup and overtopping/overwashing. Polidoro et al. (2018) observed that a swell percentage greater than 20% could have a larger impact on the elevation of the beach crest than the horizontal displacement of the beach, which may be equally applied to a barrier beach.

Through detailed, in-depth analysis using a large synthetic database the morphodynamics of gravel barrier beach (HCS) has been studied and the responses of the HCS have been quantified through parametric analysis. The aims set out at the start of this thesis were to provide an easy to use, fast parametric model for coastal management practitioners, that builds on previous parametric models (Powell, 1990; Bradbury, 2000).

.

7. Conclusions and Recommendations

The aims of this thesis were to i) develop a parametric model to capture morphodynamic response of gravel barrier to extreme conditions and ii) investigate the impacts bimodal wave conditions have on response of gravel barriers. This study uses an extensive set of numerically simulated gravel barrier beach volume change, overwash data and crest change, to investigate the response of the barrier to unimodal and bimodal storm wave conditions. The results were generated from a calibrated and validated 1D XBeach non-hydrostatic model to Hurst Castle Spit barrier beach. The results were then used to develop a simple parametric model for barrier volume change during storms. The overwash parametric model and crest change parametric model were both incomplete requiring further research and development. The overwash volumes and barrier volume change under bimodal wave conditions were compared with those from unimodal conditions.

The uncertainty of input parameters used in process-based models such as XBeach have been addressed and significantly reduced because of to the extensive synthetic database developed. The issues of previous empirical models not capturing the morphodynamics of barriers has also been improved, with the study providing quantifiable morphodynamic responses. Using this dataset, a parametric model (Eq. 6.5) was developed that can capture, within 95% confidence, the volume change of Hurst Spit to extreme conditions. The model implements a simple, yet effective set up requiring only 4 parameters - the pre-storm Barrier cross sectional area, Ba, Crest elevation, Zc, and incoming storm Hs, Tp and tide elevation + surge - which are widely available, for free, thanks to extensive network of wave buoys and tidal gauges in the UK. This enables coastal management to make time efficient, accurate initial estimates for assessing vulnerable sections of HCS. This will enable cost effective and timely coastal management decisions to be made.

Equations 6.8 and 6.10 make initial attempts to further quantify specific responses of HCS offering a more thorough and detailed estimation of barrier response to storms. The study of bimodal impacts has highlighted the wide ranging impacts bimodal conditions have on morphodynamic estimations. Bimodal results open up a route for future study and detailed investigation following a similar method used when developing the unimodal parametric models in this study. The following conclusions were drawn from the results:

- The XBeach non hydrostatic model is capable of simulating barrier volume change and overwash volume at HCS. The model was able to capture swash dynamics, sediment movement, barrier face erosion, crest build-up and back barrier sediment accumulation correctly;

- The simple parametric model derived using the numerically simulated barrier volume change has proven to be a useful tool to determine barrier response to storms. The comparison of the model with measured barrier volume change during a collection of storms at two gravel barrier beaches shows promising results;

- Bimodal waves with large swell percentages lead to greater barrier volume change and larger overwash volumes. This can be explained by the action of low steepness, high energy wave propagation on the slope of the barrier giving rise to higher runup and sediment movement on the face of the barrier. This result is in good agreement with higher wave overtopping on seawalls from bimodal seas than from unimodal seas, as found by Orimoloye et al. (2019, 2020); the larger impacts of bimodal storms on gravel barriers highlights the challenges they pose on coastal management and estimations of gravel beach response to storms. 30-40% swell component was also found to be the transition range for bimodal conditions producing greater barrier response than unimodal conditions.

- Following limitations of the approach are noted: Further validation of the parametric model is necessary for application of it into a wide range of gravel barriers; the numerical simulations were done in 1D where the impacts of longshore transport was not taken into consideration; sea level change due to global warming is not considered in the simulations, which will potentially be an important factor for determining barrier response to future storm conditions; and the model may not be applicable for bimodal storm conditions. The model is limited to storm durations of 20 hours, therefore the model may overpredict shorter storm durations or underpredict longer storm conditions.

- The model can be a very useful tool to determine initial estimates of barrier change for coastal management purposes. Using a large data base the model was able to predict within 95% confidence volumetric changes of the barrier. Using the model as an initial estimate to identify vulnerable sections of HCS will enable coastal management to carry out further detailed investigation into these sections.

7.1 Recommendations for further Study

During this study although a large number of numerical simulations were carried out more realisations with further varied input wave conditions will result in a more accurate parametric model. One limitation is that the duration of all storms are fixed at a constant 20hrs, which is the average storm duration calculated by the wave data. Therefore the model may have the tendency to overpredict barrier volume change and overwash from storms with shorter durations and underpredict those from storms with longer durations. Whilst storm duration was beyond the scope of this paper, Williams et al., (2015) showed that storms sustained over longer time periods can have a significant effect due to multiple high tide elevations occurring.

Several key parameters were evaluated in this project, with others, considered to be less important and were excluded from the study. Other models (Powell, 1990) included sediment diameter as a key variable. By including varying sediment diameters, sediment transport and the different hydraulic gradients would be encompassed in the model making it more widely applicable to other gravel beaches throughout the South West. Donnelly (2007) found that foreshore slope has an impact on morphodynamics.

Due to time restrictions, the numerical simulations of overwashed water volumes and flood floor hydrodynamics, which is important for flooding is not investigated further.

Bimodal wave conditions showed very interesting results and further study into those will be of great interest to coastal management due to the high occurrence of bimodal swell in the south-west of the UK. The range of conditions modelled were limited in comparison to unimodal cases. To further investigate the effects of 'positive' and 'negative' swell effects on barrier volume change and overwash, the range of conditions should be extended to multiple cross sections, all six extreme sea levels, and a wider range of wave conditions. Validation of XBeachX model against bimodal storm conditions is essential prior to further bimodal studies.

8. References

Almeida, L.P., Masselink, G., Russell, P., Davidson, M. (2014), Observations of gravel beach dynamics during high energy wave conditions using a laser scanner, *Geomorphology, 228, 15-27.*

Almeida, L. P., Masselink, G., McCall, R., & Russell, P. (2017). Storm overwash of a gravel barrier: Field measurements and XBeach-G modelling. *Coastal Engineering*, *120*, 22–35. https://doi.org/10.1016/j.coastaleng.2016.11.009

Aminti et al., 2003; Aminti, P., Cipriani, L.E., Pranzini, E. (2003), Back to the beach: converting seawalls into gravel beaches. In: Goudas, C., Katsiaris, G.,May, V., Karambas, T. (Eds.), Soft shore protection.

Austin, M. J., & Buscombe, D. (2008). Morphological change and sediment dynamics of the beach step on a macrotidal gravel beach. *Marine Geology*, *249*(3–4), 167–183. https://doi.org/10.1016/j.margeo.2007.11.008

Austin, M. J., & Masselink, G. (2006a). Observations of morphological change and sediment transport on a steep gravel beach. *Marine Geology*, *229*(1–2), 59–77. https://doi.org/10.1016/j.margeo.2006.02.003

Austin, M. J., & Masselink, G. (2006b). Swash-groundwater interaction on a steep gravel beach. *Continental Shelf Research*, *26*(20), 2503–2519. https://doi.org/10.1016/j.csr.2006.07.031

Bergillos, R. J., Masselink, G., McCall, R. T., & Ortega-Sánchez, M. (2016). Modelling overwash vulnerability along mixed sand-gravel coasts with xbeach-g: Case study of playa granada, southern Spain. *Proceedings of the Coastal Engineering Conference*, *35*, 1–9. https://doi.org/10.9753/icce.v35.sediment.13

BODC (https://www.bodc.ac.uk/data/hosted_data_systems/sea_level/uk_tide_gauge_network/).

Bergillos, R. J., Masselink, G., & Ortega-Sánchez, M. (2017). Coupling cross-shore and longshore sediment transport to model storm response along a mixed sand-gravel coast under varying wave directions. *Coastal Engineering*, *129*, 93–104. https://doi.org/10.1016/j.coastaleng.2017.09.009

Bradbury, A. P., & Powell, K. A. (1993). Short-term profile response of shingle spits to storm wave action. *Proceedings of the Coastal Engineering Conference*, *3*, 2694–2707.

Bradbury (2003). Evaluation of coastal process impacts arising from nearshore aggregate dredging for beach recharge – Shingles Banks , Christchurch Bay. *Observatory, Channel Coastal Forest, New Council, District*, 1–15.

Bradbury, A., Cope, S. and Prouty, D.B. (2005), Predicting the response of shingle barrier beaches under extreme wave and water level conditions in southern England, Coastal Dynamics 2005, Reston, Virginia.

Bradbury, Andrew P. (2000). Predicting breaching of shingle barrier beaches - Recent advances to aid beach management. *Papers and Proceedings 35th MAFF (Defra) Conference of River and Coastal Engineers*.

Bradbury, A. P., and Kidd, R. (1998), Hurst spit stabilisation scheme. Design and construction of beach recharge." *Proceedings of the 33rd MAFF Conference of River and Coastal Engineers*. Vol. 1. No. 1. 1998.

Bradbury, A.P., Mason, T. E., & Poate, T. (2007), Implications of the spectral shape of wave conditions for engineering design and coastal hazard assessment - Evidence from the English Channel. *10th International Workshop on Wave Hindcasting and Forecasting and Coastal Hazard Symposium*, 1–17.

Buscombe, D. and Masselink, G. (2006), Concepts in gravel beach dynamics. *Earth-Science Reviews*, *79*(1–2), 33–52. https://doi.org/10.1016/j.earscirev.2006.06.003

Brown, S. I., Dickson, M. E., Kench, P. S., & Bergillos, R. J. (2019). Modelling gravel barrier response to storms and sudden relative sea-level change using XBeach-G. *Marine Geology*, *410*, 164–175. https://doi.org/10.1016/j.margeo.2019.01.009

Carter, A. R. W. G., Orford, J. D., Lauderdale, F., & Carter, R. W. G. (1993). *The Morphodynamics of Coarse Clastic Beaches and Barriers : A Short- and Long-term Perspective of Coarse Clastic Beaches The Morphodynamics Barriers : A Short- and Long-term Perspective*. (15).

Chadwick, A. J., Karunarathna, H., Gehreis, W. R., Massey, A. C., O'Brien, D., & Dales, D. (2005), A new analysis of the Slapton barrier beach system, UK. *Proceedings of the Institution of Civil Engineers: Maritime Engineering*, *158*(4), 147–161.

Donnelly, C. (2007). Morphologic change by overwash: Establishing and evaluating predictors. *Journal of Coastal Research*, (SPEC. ISSUE 50), 520–526.

Dubois, R. N. (1990). Barrier-beach erosion and rising sea level. *Geology*, *18*(11), 1150–1152. https://doi.org/10.1130/0091-7613(1990)018<1150:BBEARS>2.3.CO;2

Goda, Y., & Takagi, H. (2000). Reliability design method of caisson breakwaters with optimal wave heights. *Coastal Engineering Journal*, *42*(4), 357–387. https://doi.org/10.1016/S0578-5634(00)00018-3

Gharagozlou, A., Dietrich, J.C., Karanci, A., Luettich, R.A. and Overton, M.F. (2020), Storm driven erosion and inundation of barrier islands from dune to region scales, Coastal Engineering, 158, 103674.

Holthuijsen, L.H., Booij, N. and Herbers.T.H.C. (1989), A prediction model for stationary, short-crested waves in shallow water with ambient currents. *Coastal Engineering*, 13(1):23–54,

Jamal, M. H., Simmonds, D. J., & Magar, V. (2014). Modelling gravel beach dynamics with XBeach. *Coastal Engineering*, *89*, 20–29. https://doi.org/10.1016/j.coastaleng.2014.03.006

KENNETH LEVENBERG. (1944). a Method for the Solution of Certain Non-Linear Problems in Least Squares. *Quarterly of Applied Mathematics*, *2*(2), 164–168.

Lee, K. H., Mizutani, N., Hur, D. S., & Kamiya, A. (2007). The effect of groundwater on topographic changes in a gravel beach. *Ocean Engineering*, *34*(3–4), 605–615. https://doi.org/10.1016/j.oceaneng.2005.10.026

Li, L., Barry, D. A., & Pattiaratchi, C. B. (1997). Numerical modelling of tide-induced beach water table fluctuations. *Coastal Engineering*, *30*(1–2), 105–123. https://doi.org/10.1016/S0378-3839(96)00038-5

López De San, B., & Blanco, R. (2003). Dynamics of gravel and mixed, sand and gravel, beaches Notation. *López de San Román Blanco*, (May).

Lorang, M. S. (2002). Predicting the crest height of a gravel beach. *Geomorphology*, *48*(1–3), 87–101.

https://doi.org/10.1016/S0169-555X(02)00176-9

Masselink. (2014). Masselink 2014 modelling with Xbeach G. *MODELLING STORM RESPONSE ON GRAVEL BEACHES USING XBEACH-G*, (2002), 1–25.

Masselink, G., & Li, L. (2001). The role of swash infiltration in determining the beachface gradient: A numerical study. *Marine Geology*, *176*(1–4), 139–156. https://doi.org/10.1016/S0025-3227(01)00161-X

Masselink, G., Russell, P., Blenkinsopp, C., & Turner, I. (2010). Swash zone sediment transport, step dynamics and morphological response on a gravel beach. *Marine Geology*, *274*(1–4), 50–68. https://doi.org/10.1016/j.margeo.2010.03.005

Matias, A., Blenkinsopp, C. E., & Masselink, G. (2014). Detailed investigation of overwash on a gravel barrier. *Marine Geology*, *350*, 27–38. https://doi.org/10.1016/j.margeo.2014.01.009

McCall, R. (2012). modelling overwash and infilltration on gravel barriers. *Journal of Chemical Information and Modeling*, *53*(9), 1689–1699. https://doi.org/10.1017/CBO9781107415324.004

McCall, R., Masselink, G., Poate, T., Bradbury, A., Russell, P., & Davidson, M. (2013). Predicting overwash on gravel barriers. *Journal of Coastal Research*, *165*(65), 1473–1478. https://doi.org/10.2112/si65-249.1

McCall, R. T., Masselink, G., Poate, T. G., Roelvink, J. A., & Almeida, L. P. (2015). Modelling the morphodynamics of gravel beaches during storms with XBeach-G. *Coastal Engineering*, *103*, 52–66. https://doi.org/10.1016/j.coastaleng.2015.06.002

McCall, R. T., Masselink, G., Poate, T. G., Roelvink, J. A., Almeida, L. P., Davidson, M., & Russell, P. E. (2014). Modelling storm hydrodynamics on gravel beaches with XBeach-G. *Coastal Engineering*, *91*, 231–250. https://doi.org/10.1016/j.coastaleng.2014.06.007

Nicholls, R. (1985), The Stability of Shingle Beaches in the Eastern Half of Christchurch Bay,. *unpublished Ph.D. thesis, Department of Civil Engineering, University of Southampton, 468pp.*

Nicholls, R., & Webber, N. (1989). *Characteristics of shingle beaches with reference to Christchurch Bay S England*. *Proc 21st*, 1922–1936.

Orford, J. D., Carter, R. W. G., McKenna, J., & Jennings, S. C. (1995). The relationship between the rate of mesoscale sea-level rise and the rate of retreat of swash-aligned gravel-dominated barriers. *Marine Geology*, *124*(1–4), 177–186. https://doi.org/10.1016/0025-3227(95)00039-2

Orimoloye, S., Karunarathna, H., & Reeve, D. E. (2019). Effects of swell on wave height distribution of energy-conserved bimodal seas. *Journal of Marine Science and Engineering*, *7*(3), 7–9. https://doi.org/10.3390/jmse7030079

Orimoloye, S., Horrillo-Craballo, J.M., Karunarathna, H. and Reeve, D.E. (2020), Wave overtopping under uni-directional bimodal wave conditions, Coastal Engineering (in press).

Paola, C.; Voller, V. R. (2005). "A generalized Exner equation for sediment mass balance". Journal of Geophysical Research. 110: F04014. Bibcode:2005JGRF..11004014P. doi:10.1029/2004JF000274

Phillips, B.T., Broen, J.M. and Plater, A. J. (2020), Modelling mpact of intertidal foreshore evolution on gravel barrier erosion and wave runup with XBeachX.

Poate, T. G., McCall, R. T., & Masselink, G. (2016). A new parameterisation for runup on gravel

beaches. *Coastal Engineering*, *117*. https://doi.org/10.1016/j.coastaleng.2016.08.003

Polidoro, A., & Dornbusch, U. (2014). Wave run-up on shingle beaches- a new method. *HR Wallingford*, (1), 114. https://doi.org/10.5749/j.ctv11vcff7.18

Polidoro, A., Pullen, T., Eade, J., Mason, T., Blanco, B., & Wyncoll, D. (2018). Gravel beach profile response allowing for bimodal sea states. *Proceedings of the Institution of Civil Engineers: Maritime Engineering*, *171*(4), 145–166. https://doi.org/10.1680/jmaen.2018.11

Powell, K. (1990). Powell (1990).pdf. *Predicting Short Term Profile Response for Shingle Beaches*, Vol. 12, pp. 295–336.

Powell, K. A. (1989), The dynamic response of shingle beaches to random waves, Proc. 21st Int. Conf. in *Coastal Engineering, Malaga, Spain,* 1763-1773.

Roelvink, D., Reniers, A., van Dongeren, A., van Thiel de Vries, J., McCall, R., & Lescinski, J. (2009). Modelling storm impacts on beaches, dunes and barrier islands. *Coastal Engineering*, *56*(11–12), 1133–1152. https://doi.org/10.1016/j.coastaleng.2009.08.006

Roelvink, D., McCall, R., Seyedabdolhossein, M., Nederhoff, K., Dastgheib, A., 2018, Improving predictions of swash dynamics in XBeach: The role of groupiness and incident band runup, Coastal Engineering, 134, 103-123.

Ruiz de Alegria-Arzaburu and Masselink, G. (2010), Storm response and beach rotation on a gravel beach, Slapton Sands, UK, *Marine Geology* 278.1-4, 77-99.

Sallenger A.H., J. (2000). Storm impact scale for barrier islands. *Journal of Coastal Research*, *16*(3), 890–895.

Shields, I. A. (1936). *Turbulence bed-load*.

Smit, P. B., Roelvink, J. A., van Thiel de Vries, J. S. M., McCall, R. T., van Dongeren, A. R., & Zwinkels, J. R. (2010). *XBeach: Non-hydrostatic model. Validation, verification and model description.* (January), 69.

Smit, P., Zijlema, M., & Stelling, G. (2013), Depth-induced wave breaking in a non-hydrostatic, near-shore wave model. *Coastal Engineering*, *76*, 1–16.

Stockdon, H. F., Holman, R. A., Howd, P. A., & Sallenger, A. H. (2006). Empirical parameterization of setup, swash, and runup. *Coastal Engineering*, *53*(7), 573–588. https://doi.org/10.1016/j.coastaleng.2005.12.005

Thompson, D. A., Karunarathna, H., and Reeve, D. E. (2018), *An Analysis of Swell and Bimodality Around the South and South-west coastline of England*. Natural Hazards and Earth Systems Science Discussion, https://doi.org/10.5194/nhess-2018-117.

Thompson, D.A., Karunarathna, H. and Reeve, D. E, 2018, Modelling extreme wave overtopping at Aberystwyth Promenade, *Water*, 9(9), p663, 2017.

Turner, I. L., & Masselink, G. (2012). Coastal gravel barrier hydrology - Observations from a prototype-scale laboratory experiment (BARDEX). *Coastal Engineering*, *63*, 13–22. https://doi.org/10.1016/j.coastaleng.2011.12.008

Van Rijn, L. C. (1993), *Principles of sediment transport in rivers, estuaries and coastal seas*. Vol. 1006. Amsterdam: Aqua publications, 1993.

Van Rijn, L. C., Wasltra, D. J. R., Grasmeijer, B., Sutherland, J., Pan, S., & Sierra, J. P. (2003), The predictability of cross-shore bed evolution of sandy beaches at the time scale of storms and seasons using process-based profile models. *Coastal Engineering*, *47*(3), 295–327.

Van Rijn, L. C. (2007), Unified View of Sediment Transport by Currents and Waves. III: Graded Beds. *Journal of Hydraulic Engineering*, *133*(7), 761–775. https://doi.org/10.1061/(asce)0733-9429(2007)133:7(761)

Van Rijn L.C. and Sutherland, J., 2011, Erosion of gravel barriers and beaches, Proc. Coastal Sediment 2011.

Williams, J. J., Esteves, L. S., & Rochford, L. A. (2015). Modelling storm responses on a high-energy coastline with XBeach. *Modeling Earth Systems and Environment*, *1*(1–2), 1–14. https://doi.org/10.1007/s40808-015-0003-8

Williams, Jon J., de Alegría-Arzaburu, A. R., McCall, R. T., & Van Dongeren, A. (2012). Modelling gravel barrier profile response to combined waves and tides using XBeach: Laboratory and field results. *Coastal Engineering*, *63*, 62–80. https://doi.org/10.1016/j.coastaleng.2011.12.010

XBeach Manual (2015), Model description and reference guide to functionalities, Deltares. (https://xbeach.readthedocs.io/en/latest/xbeach_manual)

Zijlema, M., Stelling, G. and Smit, P. (2011), SWASH: An operational public domain code for simulating wave fields and rapidly varied flows in coastal waters, *Coastal Engineering* 58(10) 992-1012.